Chapter Title: Technological Development - Droplet as a Tool

Adrian J.T. Teo[a], Say Hwa Tan[a] and Nam-Trung Nguyen[a*].

[a] Queensland Micro- and Nanotechnology Centre, Griffith University, 170 Kessels Road QLD 4111, Brisbane, Australia

*Corresponding email address: nam-trung.nguyen@griffith.edu.au.

ABSTRACT

The high uptake of droplet microfluidics in multidisciplinary research is mainly due to its capability of being a micro-scale laboratory with high versatility in controlling each microreactor. Through the implementation of three main manipulation methods, multiple reactions can be produced and subsequently used for different applications. Droplets of a predetermined mediums are first generated. Subsequently, the coalescence of different droplets can also take place to mix different reagents. Finally, sorting of droplets according to pre-set variables are carried out, facilitating analysis of results. Each manipulation method, however, can be carried out using a variety of active control methods. These can be categorised into electrical, magnetic, thermal, pneumatic, and occasionally acoustic and optical means. Further elaborations are provided in this chapter to illustrate these methods with the repertoire of mechanisms developed for these purposes. The advancement of such techniques enables high selectivity with minimal waste of resources, reducing the carbon footprint of laboratories while concurrently pursuing science.

1. 1. Introduction

Droplet microfluidics enables experimentation and analysis of sample volumes on the order of femtolitres (10^{-15} Litres)[1], while the samples remain physically separated. The droplets can also be generated at a high rate and with monodispersity[2]. Each droplet can accordingly be used as a microreactor for individual experiments, providing high precision and accuracy. Various techniques and methods have been developed to manipulate the droplets to make the system more versatile. The common manipulation tasks are generating[3], trapping[4], sorting[5], coalescence[6], mixing[7], and lastly splitting[8] of droplets using both passive and active methods. Passive methods involve permanent structures or adjustment of operation and device parameters. Passive methods do not provide selectivity, are rigid and affects all generated droplets. Active methods introduce external energy into the microfluidic system and induce additional force for the manipulation tasks mentioned above. The actuation mechanism can be precisely controlled to target specific droplets, taking advantage of its fast response time[9-11]. As such, this chapter focuses on active controls in droplet manipulation.

Active controls in droplet manipulation mainly focus on three main manipulation tasks: generation, sorting and coalescence of droplets. Although droplet trapping is commonly used, active methods generally involve the balance of different forces to hold the droplet in its position. Active methods for droplet splitting has not been widely developed, because the passive counterparts can satisfy the majority of requirements. Active methods for droplet mixing are considered as the same for droplet coalescence. Passive methods are easier to characterize as compared with active ones. Based on these observations, droplet generation, sorting and coalescence are selected as the three main manipulation tasks for this chapter.

Droplet generation refers to the production of monodispersed droplets using two immiscible fluids. Droplets are formed through the injection of the fluids into a device with intersecting channels using a syringe pump or a pressure controller. At the intersecting junction, the two fluids develop an interface, which can be controlled passively by the pressure or flow rates of the fluids. In active controls, the energy introduced into the microfluidics system is used to adjust the force balance at the fluidic interface, which in turn adjusts the parameters of the generated droplets. The use of active modulations in droplet generation enables users to control droplet size and frequency. It has also been previously presented that the response time for an active approach is in units of milliseconds, whereas the passive approach requires several seconds or even minutes[12].

Droplet sorting is the separation of different droplets after their generation. Droplet sorting is usually done to select specific droplets from a large quantity. In active control, the energy introduced is used to push or pull the selected droplets[11]. The additional force causes the droplet to travel into a separate channel within the device. Active approaches in droplet sorting enable content-determined sorting, rather than sorting using physical properties of the droplet such as its size and density. Content-based sorting has a higher value with a broader variety of applications as it is in most cases the main criteria used for droplet selection before subsequent actions or analysis can be taken.

Finally, droplet coalescence is the merging process of two or more droplets to form a single larger droplet. Active methods induce merging through two phenomena. The first phenomenon reduces the thin film of the continuous phase between the two droplets until they are close enough to trigger the coalescence. The second phenomenon involves the generation of instabilities across the surfaces of the droplets

thereby causing the breakdown of the film between the droplets. Such active methods also enable the selective and precise addition of material into the droplet for biological experiments such as picoinjection[13-15].

1. 2. Active Droplet Generation

External energy affects the fluid-fluid interface at a junction, upsetting the equilibrium of inertial, viscous, and capillary forces. The additional energy causes the liquid finger to extend beyond the junction, subsequently forming droplets. By adjusting the amount of energy introduced, the formation frequency and the size of the droplet also change correspondingly. Zhu et al [12] provided a comprehensive review detailing the influence of the external forces on different aspects of this force balance. The review categorised the phenomena according to the type of energy. This review indicated that the energy introduced in a device may not necessarily result in a direct influence on the force balance. Instead, the influences can range widely from modifying fluid velocity and material properties to having independent effects based on the nature of the energy itself. As such, a more appropriate way to classify them would be under the type of energy or the type of active control. These classification methods have been used by Chong et al[16] for active droplet generation, and the different control methods are electrical, magnetic, thermal, acoustic, optical and mechanical. Likewise, we also categorize the different control methods following this approach. However, the mechanical section will be separated into hydraulic/pneumatic controls and piezoelectric controls, as both control methods are distinct from each other.

1. 2. 1. Electrical Control

Electric field is introduced into a device through electrodes. The electrodes are generally fabricated as part of the microfluidic device and are usually made of indium tin oxide (ITO)[17, 18] although some other methods have also been developed too for this purpose[19, 20]. These electrodes have to be positioned such that the maximum effect of the electric field used is centred around the junction, where the two fluids meet. This electric field can be generated using either direct current (DC) or alternating current (AC) sources. The difference between these two sources lies in the voltage signal. A DC source provides a constant unidirectional voltage, whereas the polarity of the AC source reverses consistently according to its frequency. Although both approaches make use of a similar control method, the resultant influence on droplet generation is relatively different.

1. 2. 1. 1. Direct Current (DC)

In DC control, a constant high voltage is applied to the dispersed phase and the droplet generation is analogous to a capacitor model, where the electric stress acting on the fluidic interface is given as[17]

$$f_e \sim \varepsilon_e E^2 \quad (1)$$

Where $E \sim V/d$ is the electric field strength (V/m), ε_e is the permittivity of the continuous phase (F/m), and f_e is the electric stress that increases with an electric voltage V and inverse of the distance between electrodes d (Pa). In this case, the effect of the DC field is based on the normal stress balance on the continuous-dispersed interface,

$$\gamma C = p + (\varepsilon_c E_{c,n}^2 + (\varepsilon_d - \varepsilon_c) E_{d,n}^2 - \varepsilon_d E_s^2) \quad (2)$$

where γ, C, p, ε_c, ε_d, $E_{c,n}$, $E_{d,n}$ and E_s correspond to the continuous-dispersed interfacial tension (N/m), the local curvature of interface, local hydrostatic pressure (Pa), electric permittivity of continuous and dispersed phases, and the normal and tangential components of the electric fields of the continuous and dispersed phases respectively. As the voltage increases, the electrically induced stress correspondingly increases up to a point where it overcomes the interfacial tension, leading to instability at the interface. The instability subsequently leads to the ejection of droplets.

A DC field allows a response time as fast as 10 μs[17]. This method can be applied to a droplet-on-demand system, where pulsed excitation can be used. This concept has been successfully demonstrated by He et al., who generated femtoliter and pico-litre volume droplets Figure 1.1. However, the main disadvantage of this method is the possible contamination of the fluids used due to erosion, as the electrodes are in contact with the fluids[22].

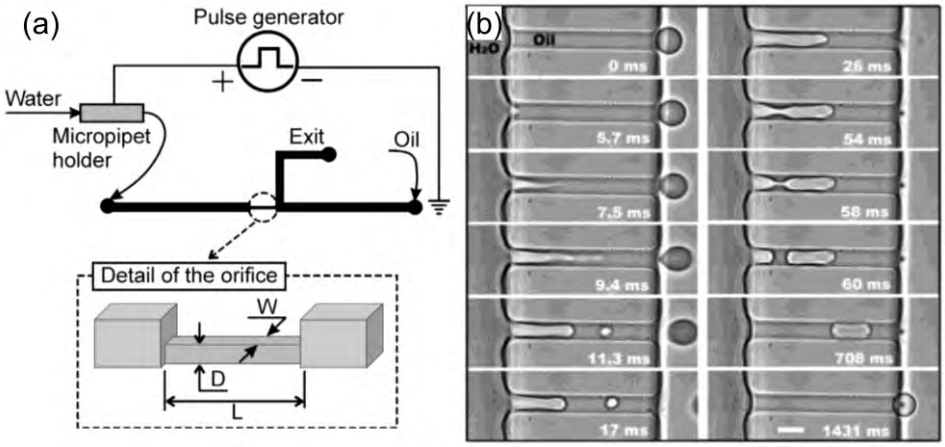

Figure 1.1 (a) Schematic diagram of the experimental setup using DC electric field (b) Image sequence showing electro-generation of a water droplet with a pulse amplitude of 1000V and pulse duration 10 ms. Scale bar represents 10 μm. Reprinted from [21] with permission from the American Chemical Society, Copyright 2006.

133

134 **1. 2. 1. 2. Alternating Current (AC)**

135 In AC control, there are two frequency ranges, relative to the frequency of
136 droplet generation. Methods working below the droplet generation frequency are
137 termed as the low-frequency approach. Methods with a frequency above the droplet
138 generation frequency are correspondingly termed high-frequency approaches. At low
139 frequencies, the droplets generated are of irregular sizes due to them being out of
140 phase with the excitation AC frequency and a hysteresis phenomenon. This mismatch
141 in frequency also results in individual droplets being unevenly charged[23]. The
142 hysteresis phenomenon can be explained by an RC electric circuit model with varying
143 resistance.

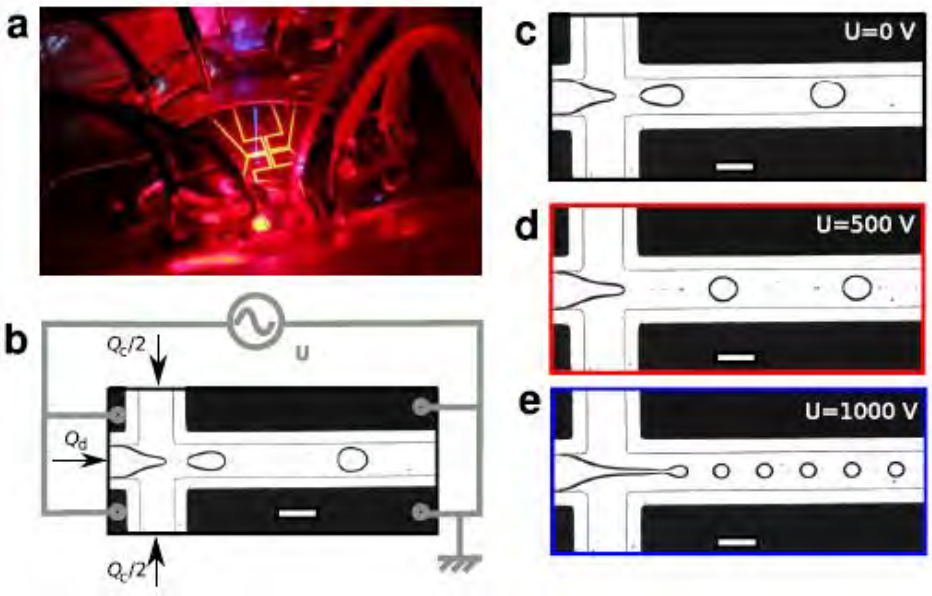

Figure 1.2 (a) Image of a microfluidic device under 473nm laser as given by the blue light. Electrodes at generation junction are seen as yellow. (b)Schematic diagram of the electrical connection for device. (c-e) Microscope image of droplet generation junction at different voltages. Reprinted from [9] with permission from Springer Nature, Copyright 2014.

For high-frequency AC fields, droplet generation is determined by the AC frequency and also the voltage applied. A paper published by Tan et al.[9] discussed the influence of both parameters on the droplet size and the generation frequency, Figure 1.2. Using a standard flow rate, experimental results suggest that the droplet size decreases in the dripping regime with an increasing voltage difference between the continuous and dispersed phase interface and the downstream electrodes. An RC circuit model was developed for his device to determine this relationship as given below[9],

$$U_{tip} = U_{app}\left(1 + \frac{1}{\frac{C_E}{C_I} + 2\pi j\left(\frac{f}{\kappa}\right)\left(\frac{C_E}{l}\right)}\right)^{-1} \quad (3)$$

where U_{tip}, U_{app}, C_E, C_I, f, κ, l are respectively the voltages at the dispersed phase interface (V), the applied voltage, the capacitance between electrodes and dispersed phase (F), capacitance between grounded indium tin oxide layer and dispersed phase, AC frequency (Hz), conductivity of dispersed phase (S/m), geometrical constant for length determined by geometry respectively, and $j^2 = -1$. Apart from this equation, another model was developed for the droplet generation in the same dripping regime as

$$Ca_{eff} = \frac{Ca}{1 - B_e} \quad (4)$$

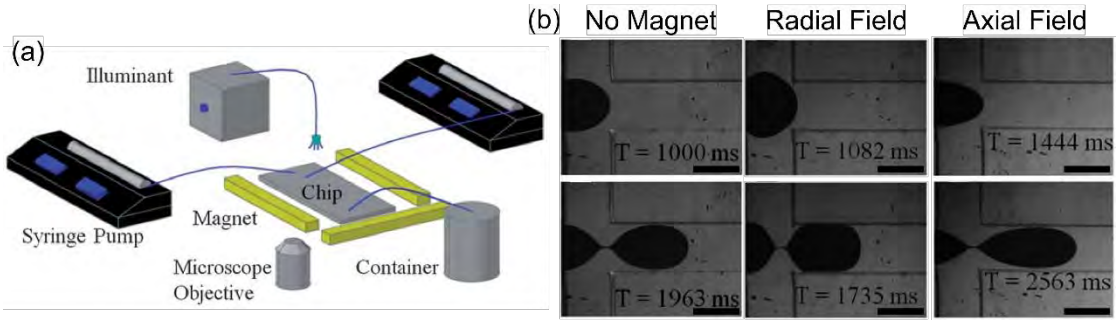

Figure 1.3. (a) Schematic diagram of the experimental setup, where magnets are added at the two sides of the chip and downstream respectively. (b-d) Microscope image of ferrofluid droplet formation without a magnetic field, radial magnetic field and axial magnetic field respectively. Scale bars are 400 μm. Reprinted and adapted from [24] with permission from the Royal Society of Chemistry, Copyright 2013.

where Ca_{eff}, Ca, B_e are separately the effective capillary number, the classical capillary number and electric bond number. Tan also successfully produced the main melody of Ode to Joy in real-time by varying the droplet generation frequency between 170 to 340 Hz[9]. His system was able to modulate the droplet generation frequency within a few milliseconds, thus making this possible.

1. 2. 2. Magnetic Control

Droplet generation using magnetic control involves the use of permanent magnets or electromagnets and ferrofluids. Ferrofluids are liquids with suspended magnetic particles with no interparticle magnetic energy. They are also superparamagnetic without magnetic memory. This means that ferrofluids can return to their original state of magnetism when there is no presence of magnetic fields[25]. Ferrofluids can either be oil-based or water-based. However, ferrofluids have only been reported to serve as the dispersed phase in droplet generation. One concern

regarding magnetic control is the usability of such droplets as the presence of magnetic nanoparticles may be unsuitable for some applications. Also, positioning the magnets relative to the droplet generation junction is paramount. In T-junctions, the droplet size increases when the magnet is placed upstream of the junction and decreases when placed downstream[26]. In a flow-focusing device, an opposite relationship between the magnetic flux density and droplet size was observed[27]. This difference is due to the orientation of the magnetic field relative to the dispersed flow direction. Under a magnetic field, the magnetic particles align with the field, which runs parallel to the main fluidic channel. In the case of a T-junction device, the alignment of the particles is perpendicular to the field, resulting in a faster breakup. Conversely, the alignment is in the same direction as the dispersed phase (ferrofluid) for the flow-focusing device, resulting in an elongated tip that delays the breakup process of the droplet. Liu et al [28] conducted a numerical study for a flow-focusing device. The model was also consistent with the subsequent experimental investigations[29]. The effects of a magnetic field in a flow-focusing device was studied and compared based on the radial and axial fields applied, Figure 1.3[24]. A radial field forms when the magnetic field is perpendicular to the flow of the droplet and the axial field is parallel. In the radial approach, it was observed that there was a perpendicular stretch in the droplet during the expansion stage of the droplet generation. This results in a larger droplet size as compared to the axial field and without a magnetic field.

1. 2. 3. Thermal Control

Droplet generation can generally be controlled through thermal means via the temperature-dependence of fluid viscosity and interfacial tension. For most fluids,

these two physical properties decrease with increasing temperature following the equation[30, 31],

$$D(T) \propto Ca_c^{-1} = \frac{\gamma(T)}{\eta_c(T)u_c} \quad (5)$$

where $D, T, Ca_c, \gamma, \eta_c, u_c$ are the droplet diameter (m), temperature (K), capillary number of the continuous phase, temperature-dependent interfacial tension, the dynamic viscosity of continuous phase (Pa.s), and characteristic speed of continuous phase (m/s^2). However, the decrease in viscosity is relatively faster than the other. As a result, the change in temperature correspondingly affects the droplet size[32]. Stan et al [31] demonstrated that an increase of two orders of magnitude was observed by increasing the temperature from 10 to 70^{o}C. The influence of temperature on the droplet generation also depends on the height of the channels used. With the smaller cross-sectional area, the thermal gradient around the generation junction is higher compared to one with a larger height[32].

Different fluids of various viscosities and interfacial tensions have also been tested and compared. In one study, the dispersed phase was changed from DI water to DI water with 15-nm spherical nanoparticles. The latter showed an 18% increase in diameter whereas the former showed a 5% increase when the temperature changed from 25^{o}C to approximately 56^{o}C[33]. Another study was conducted based on the generation of gelatin emulsions through heating of gelatin. By increasing the temperature to above 25^{o}C, the gelatin transforms into an aqueous solution with lower viscosity. This results in the release of droplets of different size and frequencies according to the temperature of the junction[34].

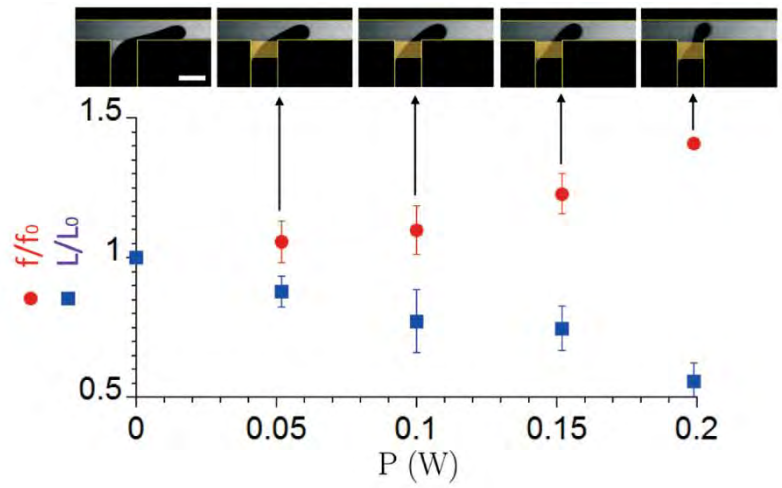

Figure 1.4. Comparison of droplet size (L/L_0) and generation frequency (f/f_0) against electric power applied to the heating resistor. Reprinted from [35] with permission from the Royal Society of Chemistry, Copyright 2015.

Another form of thermal control is localized heating at the droplet generation junction. This process is usually carried out using a focused laser beam. The laser allows for greater flexibility as it can be accurately positioned at the interface between the continuous and dispersed phase. In this manner, a localized temperature gradient is generated, resulting in a gradient of interfacial tension that induces the Marangoni effect. The Marangoni effect relates the normal component of the shear stress to the tangential derivative of temperature. The interfacial tension causes a flow in the direction away from the region of low interfacial tension, resulting in a "blockage effect" that affects the droplet size and the generation frequency. Baroud et al. [36] reported that the blocking time increased relative to the beam power used. The increasing blocking time, in turn, resulted in a larger droplet size, which is up to 1.5 times in length using beam power of approximately 70 mW. Figure 1.5 shows the influence of the laser on the droplet formation process. The Marangoni effect is also subsequently applied to droplet sorting by selectively restricting the movement of droplets into specified channels. Apart from using the laser beam, Miralles et al. [35] demonstrated

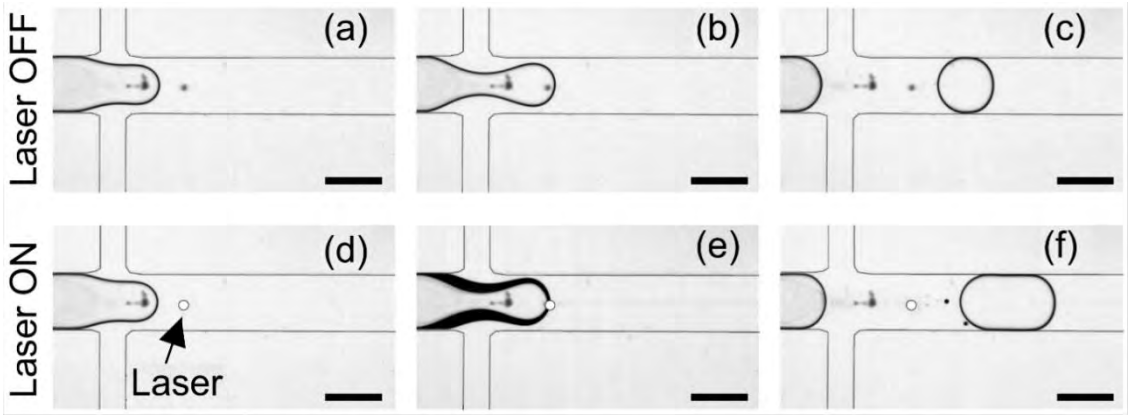

Figure 1.5. Microscope images demonstrating the effects of laser-induced droplet blocking. The interface was blocked using a laser beam to produce a large droplet. Scale bars depict 200μm. Reprinted from [36] with permission from the American Physical Society, Copyright 2007.

thermal controls using integrated heating resistors along a microchannel, Figure 1.4. The device managed to adjust both the generation frequency and droplet size by increasing the power applied to the heating resistors. On top of this, the device was also capable of carrying out droplet sorting.

1. 2. 4. Pneumatic Control

Droplet generation can be controlled by varying the flow rates or pressure values of individual fluidic phases. Mechanical valves employing hydraulic/pneumatic actuators are integrated into the devices to add a level of control. By regulating the flow rates or fluidic pressure directly, the flow condition at the droplet generation junction is correspondingly affected[37], Figure 1.6. In this way, the droplet generation can be regulated. These valves can be either off-chip[38, 39] or integrated into the device design[40, 41]. Off-chip valves directly affect the dispersed phase pressure by pulsating valves using a series of on-off signals, while the continuous phases are separately

controlled. Based on the laminar flow within the microchannels, the droplet volumes can be predicted using the equation[42],

$$V \sim \frac{\Delta P_d t_{on}}{Rre_d} \tag{6}$$

where $V, \Delta P_d, t_{on}$ and Rre_d are respectively the droplet volume (m^3), the pressure drop along the microchannel of the dispersed phase (Pa), on signal time duration (s), and flow resistance ($kg.m^{-4}.s^{-1}$) in accordance to $R_i = 12\mu \frac{L_i}{W_i H_i^3 \left(1-0.63\frac{H_i}{W_i}\right)}$ for closed rectangular microchannels. By adjusting the voltage and frequency of the on-off signal,

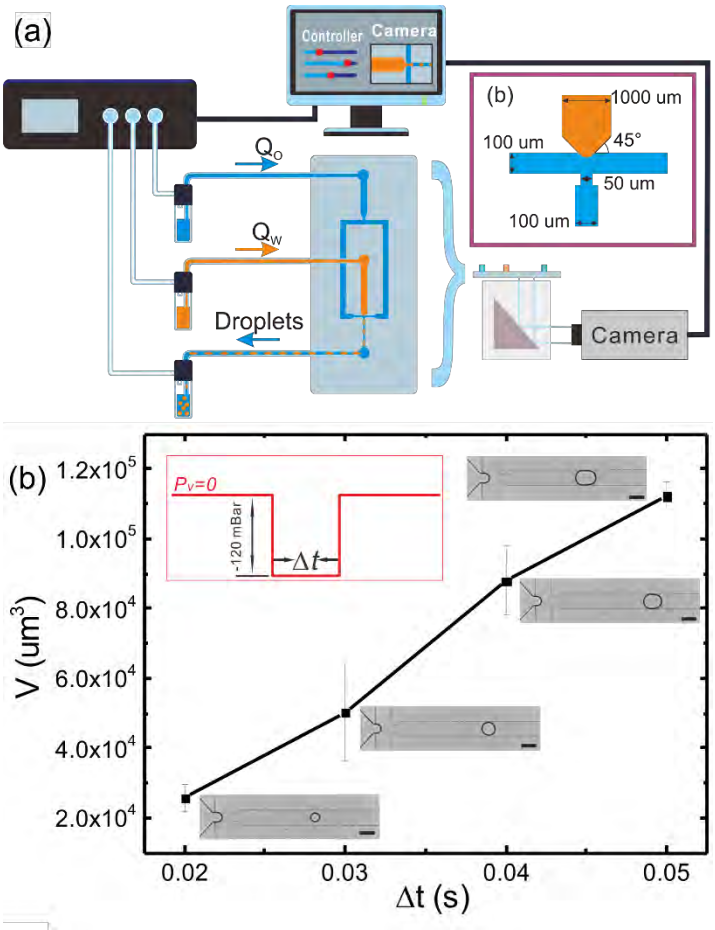

Figure 1.6. Droplet generation using pneumatic pressure controls at the outlet of the device for droplet size control. Reprinted from [37] with permission from the American Physical Society, Copyright 2017.

droplet size and frequency can be adjusted. Concurrently, droplet on demand can also be achieved[46].

On-chip valves influence droplet generation through either channel deformation[43, 44] or blocking of the channels[40]. In this approach, a thin layer of PDMS separates the actuation and fluidic channels to prevent the fluids from flowing into the wrong channel. The actuation channel can be placed either upstream[47], at the droplet generation junction[48] or downstream[45]; above[49] and below[41] the fluidic channels or along the same plane[44]. Depending on the plane of the actuation channel, a multilayer device fabrication may be needed as shown in Figure 1.7a, which is more difficult[43,

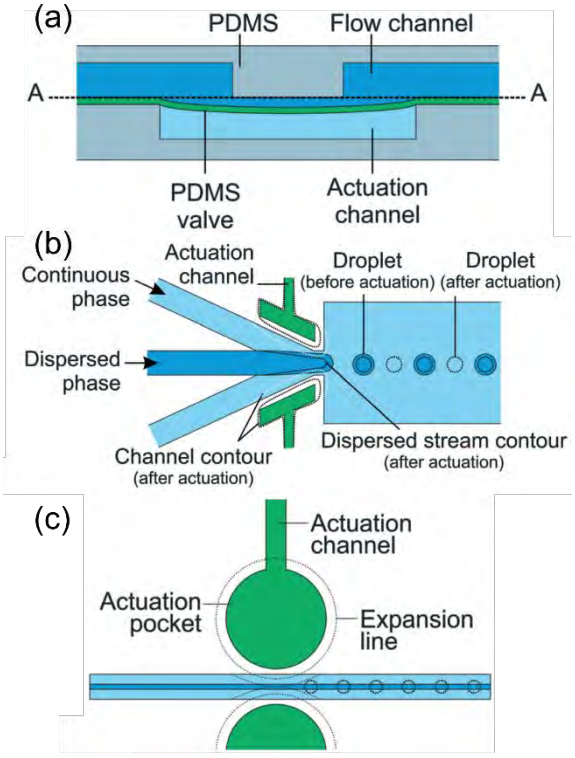

Figure 1.7. Schematic diagram of pneumatic microvalves. (a) Multilayered microvalve control size of generated droplets[43]. (b) Pneumatic valves at droplet generation junction control flow rate of fluids adjusting the sizes of droplets[44]. (c) Microvalves employing "chopping" method to generate droplets[45]. Reprinted from [16] with permission from the Royal Society of Chemistry, Copyright 2016.

[50]. If the valve is placed upstream, a perturbation effect is utilised to vary the dispersed fluid flow rate, enabling a linear decrease in volume with respect to the actuation frequency[47]. For valves located at the droplet generation junction, using a flexible membrane with an actuation that is large enough to induce intermittent flow or blocking would also generate droplets, Figure 1.7b,c. Apart from these “normally open” type of valves, “normally closed” valves have been used to open the disperse channel to release the fluid into the main fluidic channel[43]. The generation of droplets using downstream valves would typically require a two-phase parallel flow in its main microchannel. Upon the activation of the pneumatic control, the valves would break up the flow to generate discrete droplets running with high-flow-rate ratios. This is because of the stronger “chopping” forces from the valves as compared to the viscous forces imposed by the continuous phase. One drawback of this method however is that droplets that were already “chopped” and might be “chopped” again if the flow rate is not high enough compared to the actuation frequency. Apart from this, the generation frequency is also limited by the actuation frequency[45].

1. 2. 5. Piezoelectric Control

Piezoelectric actuators can be used to generate droplets. There are three approaches for piezoelectric control of droplets. The first approach is commonly used in inkjet printers. This is done through the deformation of a dispersed phase chamber to generate a pressure wave that pushes the fluid into the continuous phase. The droplet size can be determined by adjusting the duration of the driving pulse and applied voltage. A high generation frequency of 2.5kHz was observed by Xu et al. [51], who managed to produce droplets on-demand with this approach. The optimal droplet

generation frequency, however, was observed to be correlated with the natural frequency of the actuator itself. Unfortunately, no experimental results for the lifespan of this device were reported.

The second approach is using piezoelectric actuation to generate an acoustic effect on the dispersed-continuous interface. Acoustic actuation accelerates droplet breakup by imposing periodic oscillations to the interface, resulting in a periodic change in the curvature at the generation junction. The generation process was influenced at a relatively low actuation frequency. The droplet size reduced with increasing voltage and frequency due to an increase in the vibrational motion as observed using micron-resolution particle image velocimetry (μPIV)[52, 53].

The third approach is generating surface acoustic waves (SAW) across the microfluidic device. SAW is generated through applying an AC voltage on a pair of interdigitated transducers (IDT) deposited on a piezoelectric substrate. The AC voltage causes the piezoelectric material to generate a mechanical wave that travels across the substrate. As the wave travels across the surface, the amplitude decays exponentially along the normal direction of the substrate. This travelling wave transfers the acoustic energy into the dispersed-continuous interface, pushing the fluids in the direction away from the electrode along the crystallographic orientation of the substrate. Droplet size can be modified by adjusting the applied power and pulse duration[54]. By activating the IDT in front of the continuous phase channel at the generation junction of a flow-focusing device, the generated SAW causes an asymmetric excitation of the thinning neck at the break-up stage of droplet generation. This process reduces the time taken for the break-up. When placed further away from the T-junction, the droplet size decreases with increasing acoustic power[55]. This phenomenon made use of the pressure increase that is induced due to the presence

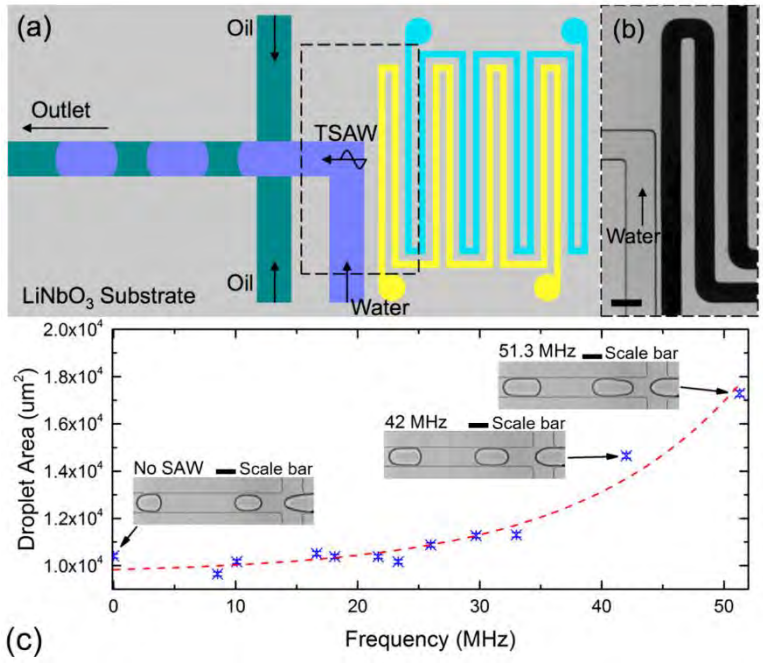

Figure 1.8. A device employing piezoelectric controls. (a) Schematic of SAW-modulated droplet device. (b)Microscope image of an electrode placed beside fluidic channel. (c) Relationship between the droplet area and acoustic frequency chosen. Reprinted from [57] with permission from MDPI, Open Access.

of the SAW. However, the increase is non-linear, with the pressure increasing almost twice the expected value at a higher SAW power. Apart from the conventional designs for the electrodes, a set of focused IDTs was developed by Collins et al. [56], where droplet on demand was also displayed. A relationship between the droplet area and acoustic frequency applied was also observed by Ma et al [57], Figure 1.8. Acoustic streaming was hypothesized to be the cause for this increase in droplet area.

1. 3. Active Droplet Sorting

According to the Merriam-Webster dictionary, the definition of "sort" is given as "to arrange accordingly to characteristics". Droplet sorting, therefore, is a process of separating droplets according to a specific criterion. Sorting of droplets and particles are highly desirable especially from a large population as it allows greater efficiency in high-impact applications such as in the generation of high throughput biological assays [2, 58] and research on enzymatic activity[59]. These applications are mainly based on sorting according to contents rather than hydrodynamic properties[60, 61]. Apart from this, active sorting also offers higher efficiency and throughput. Droplet sorting can be categorised into five main controls - electric, magnetic, thermal, pneumatic and acoustic control - as observed in Figure 1.9. The different approaches in active droplet sorting are later discussed concerning closed-channel droplet-based microfluidics.

1. 3. 1. Electrical Control

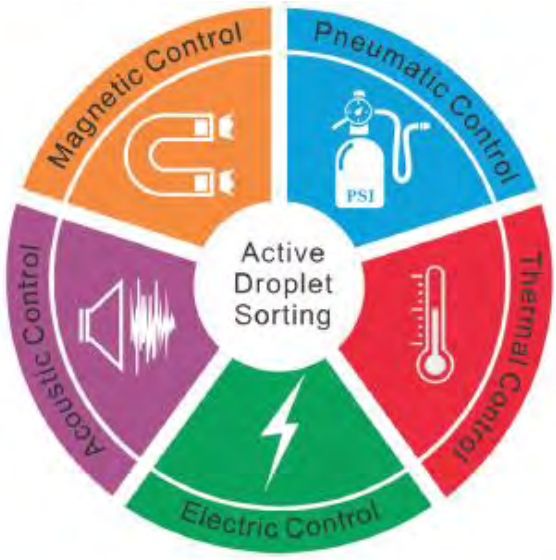

Figure 1.9. Classification of different active sorting methods. Reprinted from [11] with permission from the Royal Society of Chemistry, Copyright 2017.

Similar to droplet generation, electric controls in droplet sorting also involve the use of electrodes to produce an electric field to influence the droplet. Likewise, this actuation method also boasts the same fast response timing for use in high throughput scenarios. However, one main difference is in the positioning of the electrodes. The electrodes in this case have to be placed downstream near the junction between the sorting channel and the waste channel, away from the droplet generation junction. Proper arrangements must be in place to restrict the influence of the electric field on the fluidic channel. Some examples would be to either place a "moat" [62, 63] or to design sharp electrodes[64].

Droplet sorting using electric controls generally involves the action of either a push or pull on a droplet due to the pre-charging of droplets[65] or the difference between the electrical conductivities and/or permittivity between the dispersed and continuous phases. This method of control does not apply to all fluids. Instead, different combinations of fluids would produce different results, restricting their choice. Also, not all applications are suitable because of the need for charging. However, this control method still proves to be highly effective as many users employ it in their devices. The electric fields are either direct current (DC) or alternating current (AC) as elaborated further below.

1. 3. 1. 1. Direct Current (DC)

The use of a DC field in droplet sorting is often linked to the need for pre-charging of droplets[17, 65, 66]. Pre-charging requires an additional set of electrodes to be placed before the sorting junction. The droplets also need to be in direct contact with

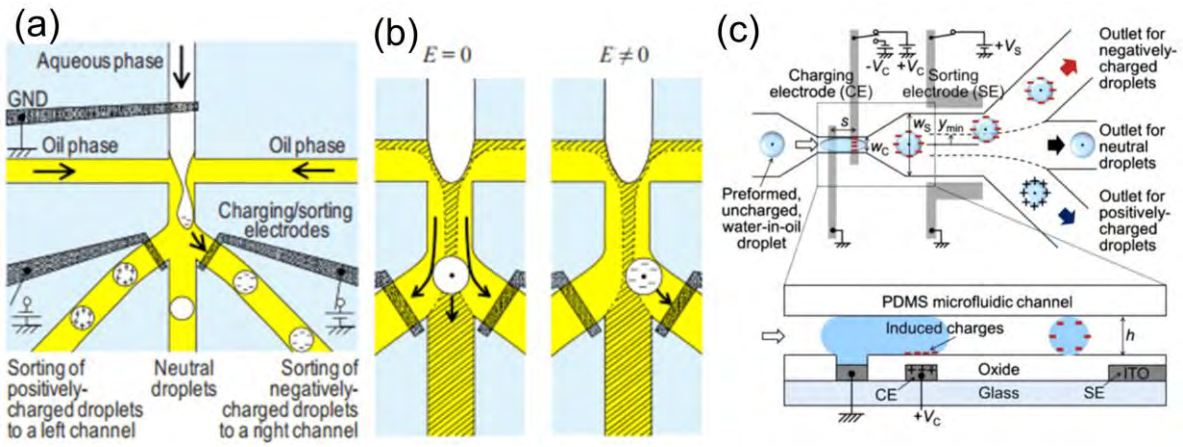

Figure 1.10. (a-b) Schematic diagram of concurrent droplet charging and sorting. Droplets are charged upon generation and subsequently steered into designated channels according to the charge of the channel[66]. (c) Schematic diagram of improved version of device employing DC electric field[65]. Reprinted from [65, 66] with permission from AIP Publishing, Copyright 2009, 2011.

the electrode, risking electrode fouling and short-circuiting if carried out incorrectly. The force experienced by the charged droplet in this case is

$$F_E = qE \tag{7}$$

and

$$E = \frac{V}{d} \tag{8}$$

where q, E, V and d are respectively the charge on the droplet (C), applied electric field, applied voltage, and distance between the electrodes (m).

Ahn et al. [66] developed a device (Figure 1.10a,b), in which the dispersed phase is first grounded using an electrode. At the droplet generation junction, a branch of three microchannels was used, with two electrodes of different charges over two separate channels. By turning on each electrode separately, the interface of the liquid

finger gets charged accordingly and the generated droplet retains the charge. The droplet then goes into its correspondingly charged channel. Sorting rates of 600 droplets/sec were achieved using this approach. A further improvement of this method was developed in 2011, where preformed uncharged droplets were charged and subsequently sorted as presented in Figure 1.10c[65]. In this device, only the two charging electrodes were in contact with the fluids, slightly reducing the risk of fouling. The sorting electrode also shifted right before the sorting channels in this modification. In this configuration, the total force acting on the droplet is given as

$$m\frac{d^2y}{dt^2} = F_{Electric} + F_{Drag} = qE - 6\pi r\eta\frac{dy}{dt} \quad (9)$$

where m, y, t, r, η are the mass of the droplet (g), deflection of the droplet in the perpendicular direction from fluid flow direction, travelling time of droplet along sorting electrode (s), the radius of the droplet (m) and dynamic viscosity of continuous phase. By using this equation together with Equation 8, the voltage needed for the sorting can be determined. Droplets can be electrostatically charged to be positive or negative in this approach but the droplet has to be in contact with both charging electrodes at the same time. This means that a minimum droplet diameter is required, which is

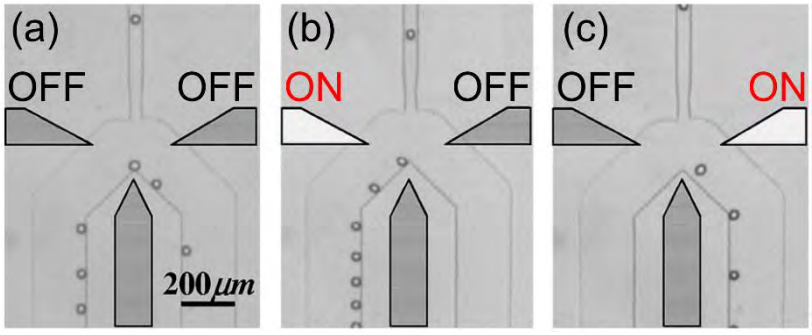

Figure 1.11. Effect of AC electric field on monodispersed droplets: (a) Without electric field (b) Left electric field on, (c) Right electric field on. Adapted from [64] with permission from AIP Publishing, Copyright 2006.

386 determined by the charging electrode spacing. Droplet sorting was observed to only
387 be successful within specific flow rate ratios and droplet sizes.

388

389 **1. 3. 1. 2. Alternating Current (AC)**

390 The working mechanism behind the use of AC electric fields in droplet sorting
391 is dielectrophoresis (DEP). DEP is the motion of polarizable objects such as particles
392 and cells caused by the application of a non-uniform electric field. The force behind
393 this is clearly defined by Pethig et al [67]. A simplified version is given as[64]

394 $$\vec{F} = \vec{m} \cdot \nabla \vec{E} \tag{10}$$

395 where $\vec{m}$ is the dipole moment of a particle (Nm) and $\vec{E}$ is the electric field. The induced
396 dipole moment of a spherical particle is subsequently

397 $$\vec{m} = 4\pi\epsilon_c Re[CM(\omega)]r^3\vec{E} \tag{11}$$

398 where ϵ_c and r are the dielectric constant of the continuous phase, and the radius of
399 the particle. $Re[CM(\omega)]$ is the Clausius-Mossotti factor which is equivalent to 1 for
400 water in oil droplets at frequencies up to several MHz. The dielectric force is
401 subsequently balanced by the viscous force, also called Stokes drag,

402 $$\vec{F_s} = 6\pi\eta_c r\vec{v}, \tag{12}$$

403 where η_c and $\vec{v}$ are the viscosity of the continuous phase and velocity of the droplet.
404 Ahn et al [64] reported one application of this method, where droplets of different
405 diameters and velocities were investigated. An AC voltage of up to 2kV was applied
406 across the electrodes as shown in Figure 1.11a-c. The maximum rate of droplet sorting
407 depends on the force generated by the electric field gradient, which also determines

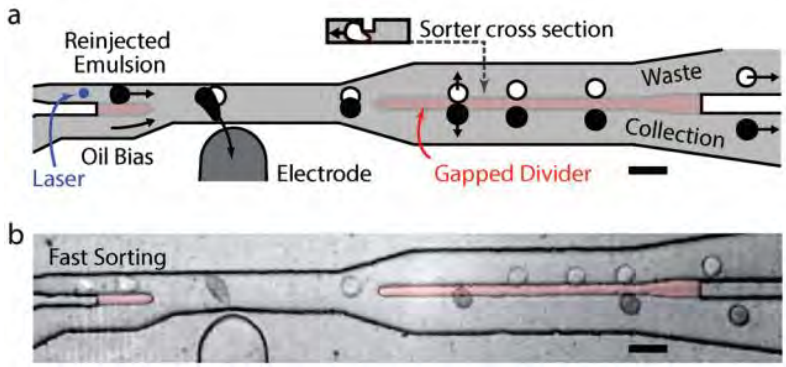

Figure 1.12. (a) Schematic drawing of the sorting junction with the black droplets being sorted. (b) Image obtained from high-speed video showing 22kHz sorting. Scale bars denote 50μm. Reprinted from [62] with permission from the Royal Society of Chemistry, Copyright 2015.

the terminal speed of the droplets. The sorting rate was limited by the time required for the electric field to displace the drops to a distance away from the centre streamline. Pethig et al reported that a sorting rate of 4kHz was achieved without optimization. Bidirectional sorting was also accomplished by energizing opposite electrodes as given in Figure 1.11a-c.

Another device using DEP forces managed to successfully sort droplets at a high frequency of 30 kHz[62, 63]. This device made use of a gapped divider that was one third the height of the microchannel placed approximately 220 μm away from the electrode, Figure 1.12. The usage of the gapped divider allows droplets to squeeze into the tight gap where the small lateral displacements from the DEP is magnified with the aid of the droplet Laplace pressure as it travels down the channel. The results showed a 99.3% sorting efficiency for the positively sorted droplets.

1. 3. 2. Magnetic Control

Magnetic controls in droplet sorting allow for wireless control of droplets similar to drug delivery in the biomedical field[68]. The same approach of using magnets on ferrofluids or droplets with magnetic particles was mentioned earlier in the previous section for droplet generation. Likewise, the same disadvantage remains that the presence of magnetic materials within the droplet may not be suitable for many applications. There are two approaches in this category: using an electromagnet or a permanent magnet. An electromagnet allows sorting on-demand with easily adjustable field strength, but heating of the device would occur due to the electric current. Heating could affect the fluidic properties or the chip itself adversely. The use of a permanent magnet, on the other hand, does not provide any switching capabilities and would constantly be applied in the device. However, a permanent magnet does not cause any adverse effects on the chip or fluidic environment. The strength of the magnetic field can also be adjusted according to the positioning of the magnet from the device.

Magnetic guidance and parking of droplets were demonstrated by Teste et al. [69] using an electromagnet. Magnetic rails were fabricated into the PDMS substrate to serve as guides to direct the droplets mixed with magnetic beads. Although there was no mention of sorting frequency, the method proves to be a viable concept for droplet sorting at low frequencies. Another device developed by Zhang et al. [70] makes use of a movable permanent magnet for sorting of superparamagnetic droplets into three channels. In this approach, superparamagnetic droplets and nonmagnetic water droplets were flowed into the device as shown in Figure 1.13. The magnetic force, F_m, acting on individual magnetic droplet is given as

$$F_m = \frac{N \cdot \Delta\chi \cdot V}{\mu_0} \cdot B \cdot (\nabla B), \tag{13}$$

where $N, \Delta\chi, V, \mu_0, B$ and ∇B are number of magnetic nanoparticles in each droplet, the difference in magnetic susceptibility between the nanoparticle and buffer used, the volume of particle, permeability of vacuum ($4\pi \times 10^{-7}$H/m), magnetic flux density (T) and magnetic field gradient. As the droplet would be deflected from laminar flow, a drag force, F_s, would be observed similar to Equation 12 given above. To reach an equilibrium,

$$F_m = F_s \tag{14}$$

Considering the deflection angle of the superparamagnetic droplet and putting the equations together, the following relationship is obtained,

$$\tan(\theta) = \frac{v_y}{v_x} = \frac{2C \cdot \Delta\chi \cdot r^2}{9\eta \cdot \rho \cdot \mu_0 \cdot v_x} \cdot B \cdot (\nabla B), \tag{15}$$

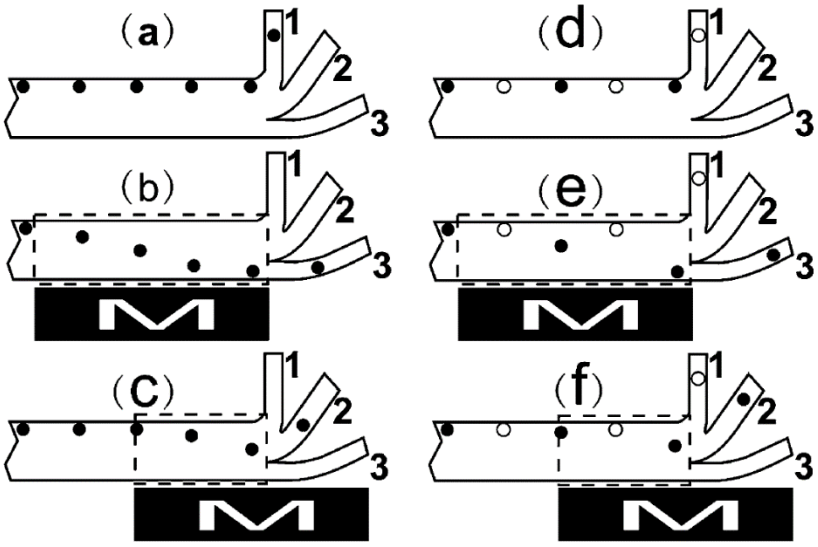

Figure 1.13. (a-e) Schematic diagram of droplet sorting using superparamagnetic droplets in black and nonmagnetic water droplets in white. Superparamagnetic droplets are drawn into different channels based on the positioning of the magnet as provided. Reprinted from [70] with permission from the Royal Society of Chemistry, Copyright 2009.

where θ, v_y, v_x, C, r, ρ are the deflection angle (degrees), velocity component in the y and x-direction, concentration, radius and density of droplet (kg/m^3). For the experiments, droplets are flowed such that they are on the opposite side of the fluidic channel with reference to the magnet. The normal water droplets would enter channel 1 in Figure 1.13c, however, the superparamagnetic droplets would be drawn to the magnet and sorted into channel 3, Figure 1.13d. By shifting the magnet to the right, the superparamagnetic droplet then changes to enter channel 2, Figure 1.13e. This is determined to influence the ∇B which is weaker outside the controllable region that is the area perpendicular to the magnet surface. Different magnetic field gradients and nanoparticle concentrations were varied and matched well with the theory suggested.

1. 3. 3. Thermal Control

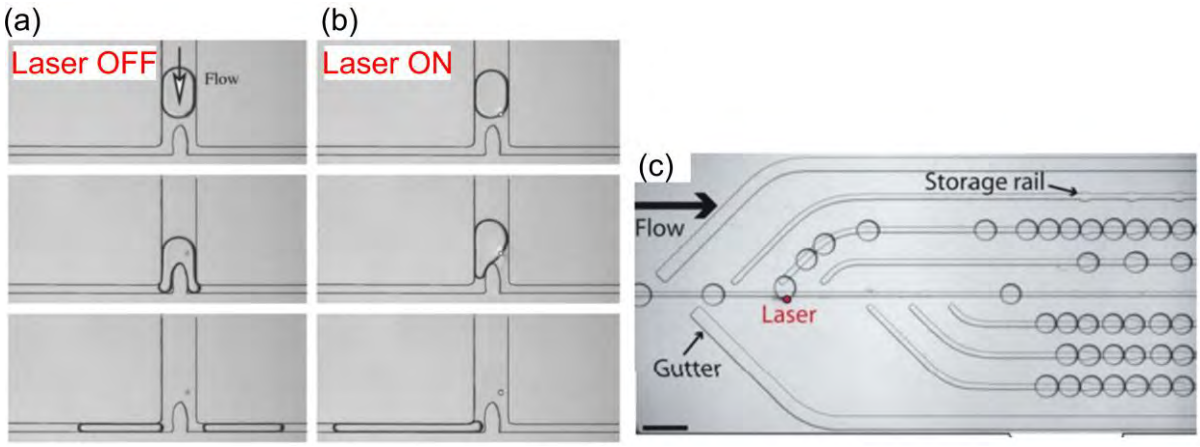

Figure 1.14. Microscope images of droplet sorting using laser. (a-b) Laser beam used to block channel entrance using thermocapillary forces. Reprinted from [36] with permission from the American Physical Society, Copyright 2007. (c) Laser beam used to sort droplets into different storage rails. Reprinted from [71] with permission from the Royal Society of Chemistry, Copyright 2011.

Thermal controls are developed based on thermocapillary effects. There are two kinds of thermocapillary effects depending on how the interfacial tension changes as a function of temperature, i.e. attractive thermocapillary effects or repulsive thermocapillary effects[72]. Attractive effects occur when the interfacial tension decreases with increasing temperature and repulsive effects have the opposite effect. For most fluids, attractive capillary effects usually take place. However, through the introduction of surfactants, the repulsive effects become more prominent as a result of the increase in molecular cohesion due to chemical properties[73]. Thermocapillary effects can be induced in a microfluidic device using two means. One is attaching heaters on the chip itself, another is through a focused laser beam. Resistive microheaters were first reported by Yap et al. [74], where the heater was positioned right below the downstream of the fluidic channel. A sensor was integrated to determine the temperature within the channel itself. By increasing the temperature at one branch, the heater created a high temperature gradient at the lower branch. The high temperature results in a drop in viscosity and interfacial tension, increasing thermocapillary effects[72]. At a temperature of 40°C, the droplet was observed to only travel through the lower branch displaying attractive thermocapillary effects. However, there was no mention of any droplet sorting on demand capabilities.

The application of lasers on droplets has been widely studied by various researchers[75-77]. For droplet sorting, a focused laser beam provides highly localized heating with high flexibility in positioning while also enabling sorting on demand. By placing the laser in front of a channel, a resistive thermocapillary effect can be induced, which blocks the droplet from entering the channel as given in Figure 1.14a,b [36 , 71, 78]. The laser power required for this effect to take place was observed to depend on the ratio of h/R and w/R where h, w and R are the height of the channel, width of the laser

492 hotspot and radius of the droplet respectively[36] . Another sorting method employing
493 the use of laser-induced thermocapillary effects is reported by Fradet et al [71]. This
494 method takes advantage of the flexibility of positioning of the laser beam to sort
495 droplets into a series of storage rails, Figure 1.14c. This method allows droplets to be
496 sorted into multiple channels in-situ, however, there is a risk of droplets being in
497 contact with one another, causing contamination, especially for biological specimens.

498

499 **1. 3. 4. Pneumatic Control**

500 Pneumatic controls in droplet sorting can be done mainly through two means.
501 One is adjusting the flow within the device using a separate pressure source, while the
502 other is using in-built microvalves or microactuators.

503 **1. 3. 4. 1. Flow control**

504 For the former, a common approach is to have a separate channel for the sorter
505 fluid, which would usually be the same as the continuous phase fluid used. Sorting is
506 determined by the activation of a sorter fluid. Upon detection of a droplet with desired
507 criteria, a pulse signal is sent from the controller to the actuator or valve for the sorter
508 fluid. This subsequently results in a momentary change in the pressure exerted by the
509 sorter fluid. A positive pressure would push[79-81] the droplet into a collection chamber,
510 and negative pressure would pull[82, 83] the droplet in. By generating square pulsed
511 positive pressure of approximately 70mBar with a duration of 7ms, Cao et al. [79]
512 developed a device that would be able to sort two-bead droplets up to 55 Hz, Figure
513 1.15. In another device by Shemesh et al. [80], the device was able to sort according to
514 droplet volume, droplet content and also sort densely packed droplets into clusters.
515 The versatile method of sorting was carried out using a triangle pulse signal for the

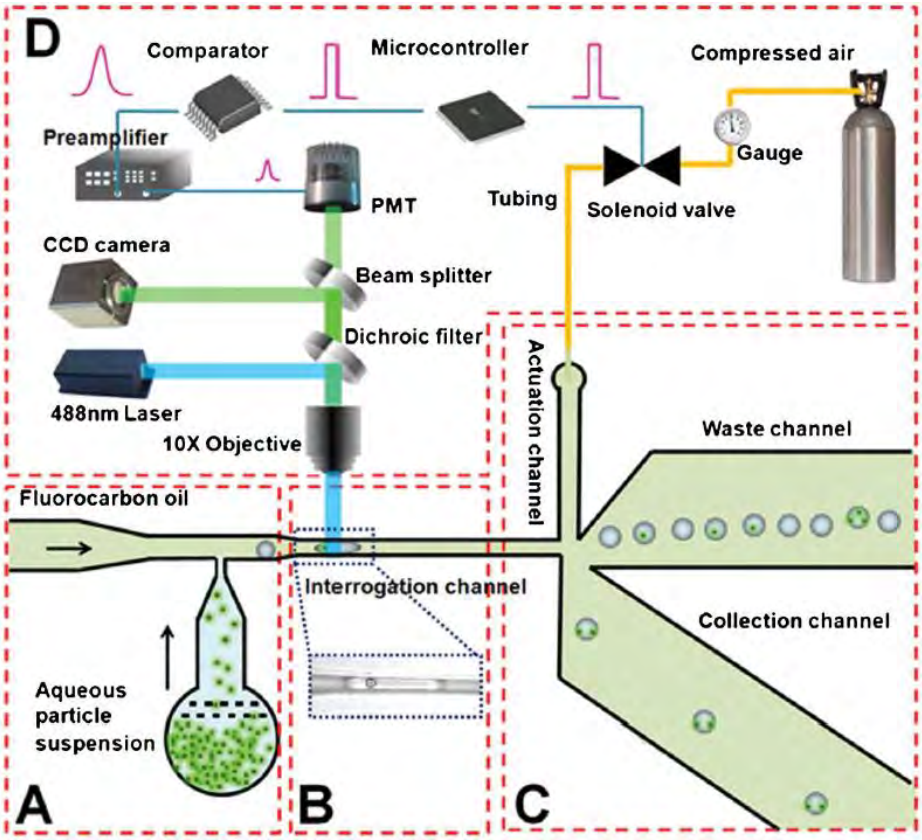

Figure 1.15. Schematic diagram of the droplet sorting system with an actuation mechanism connected to an air tank via a solenoid valve for sorting. Reprinted from [79] with permission from the Royal Society of Chemistry, Copyright 2013.

sorter fluid. The sorting outlet was not placed directly in front of the collection chamber to minimize shear stress. Also, the length of the side channel was increased to prevent undesired sorting. Although this device is well designed and versatile, the maximum sorting rate achieved, however, was relatively low at 5Hz. The use of negative pressure has also been reported by Zhang et al. [82] who was able to carry out on-demand droplet sorting up to 10Hz. Another novel application of negative pressure in droplet sorting is carried out by Wu et al. [83]. This approach employs a T-junction at the sorting junction where the sorter fluid works similar to Shemesh's device. However, negative pressure was used in this case at the collection chamber and waster chamber for sorting. With this method, pressures at both channels had to be optimized to allow

adequate hydrodynamic gating while allowing adequate droplet generation. A high sorting rate of above 98% was reported using this method.

1. 3. 4. 2. Microvalves

The use of microvalves in droplet sorting involves the deformation of channel walls to block or restrict the flow within a microchannel. This restriction increases the flow resistance, resulting in the movement of the droplet into a second channel. Similar to droplet generation using microvalves in the previous section, these devices have a common disadvantage of not being long-lasting and are highly dependent on substrate flexibility. These valves can also be fabricated using multilayered or single-layered fabrication depending on the placement of the valves. Multilayered ones, however, add a disadvantage due to its fabrication complexity. Chen et al. [84] developed a device with microvalves fabricated on top of two control channels. In his approach, the detection of an arriving droplet would prompt the controller to send a signal to pressurize either valve. When the droplet enters the sorting area, the pressurized valve would release, resulting in a drawing force on the droplet into the sorting channel along the same side of the channel. Although the sorting mechanism was not mentioned, the device was shown to be able to sort alternating droplets into separate channels. Sorting efficiency was also almost 100% at low frequencies up to 20Hz.

Single layered microvalves developed were mainly positioned at the sorting junction. In 2008, Abate et al. [85] developed a device with a single microvalve placed right after a sorting junction. To optimize the performance of the valve, the relationship between the pressure drop (Δp) along a microchannel and other critical parameters was developed as such

$$\Delta p \propto \frac{vl}{hw^3}, \tag{16}$$

where v, l, h and w are the fluid flow rate (L/hr), valve head length, channel height and width (m). The amount of crosslinker for the substrate material was also varied to determine the influence of each parameter on the performance of the valve. Based on the experimental results, it was observed that a device with 6.3% crosslinker concentration, 100μm height, 10μm channel width and 1000μm length would produce the greatest drop in pressure. This device was reported to have a fast response time however there was no mention of the sorting frequency. Also, as the length of the valve head is large, it would be impossible to achieve single droplet sorting. Subsequently, more devices developed using this method made use of the smaller valve length[87, 88]. In 2015, Yoon et al. [86] proposed a new design making use of the

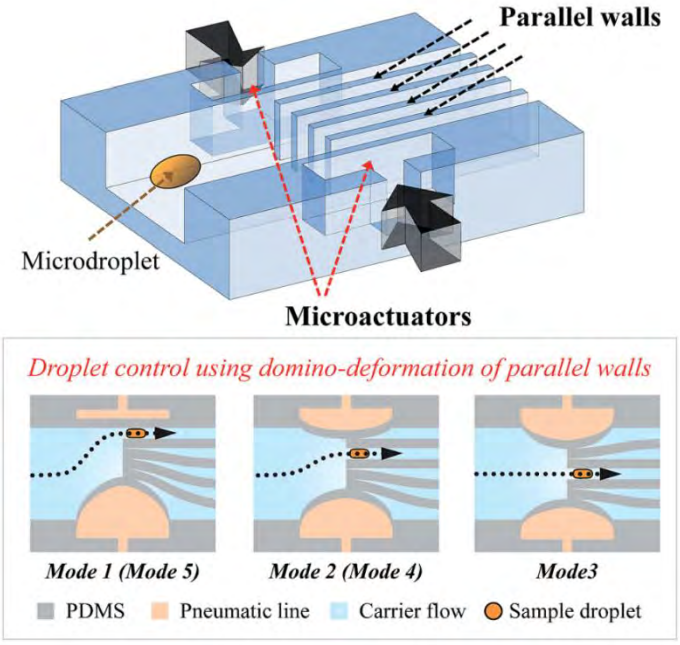

Figure 1.16. Schematic diagram of the fluidic junction using the domino effect of parallel walls for droplet sorting. Pneumatic actuation using single-layered microvalves are used to deform channel walls. Reprinted from [86] with permission from the Royal Society of Chemistry, Copyright 2015.

561 domino deformation of parallel walls for sorting, Figure 1.16. Similar to other devices,
562 this device first uses microvalves to block the main channel to enable the droplet to
563 move down towards the sorting channels. Following that, another set of microvalves
564 are used to squeeze the walls of the collection chambers to reveal an opening for the
565 droplet to enter. This device was able to sort droplets into five different chambers.
566 However, the concept magnifies the problem with all microvalve devices, which is the
567 short lifespan of the device. The device could only withstand 100 cycles and only
568 lasted for less than 2 hours.

569

570 **1. 3. 5. Acoustic Control**

571 The application of acoustic controls in droplet sorting relies on the use of
572 interdigitated transducers (IDT) on a piezoelectric substrate, similar to the ones used
573 for droplet generation mentioned earlier. Likewise, AC voltage is applied to a pair of
574 transducers causing the piezoelectric material to generate mechanical waves that
575 travel across the substrate in a direction-dependent on its crystallographic orientation.
576 This wave is called a surface acoustic wave (SAW). Another type of acoustic wave
577 that is used for sorting is the bulk acoustic wave (BAW), which travels through a
578 medium instead of the surface. Acoustic streaming (AS) and acoustic radiation forces
579 (ARF) are commonly observed through the usage of this control method. In AS,
580 acoustic energy is radiated into fluids from SAWs due to the sound velocity mismatch
581 between these two mediums. The induced pressure wave results in a steady-state
582 flow generated within the fluid itself which scales according to the ratio of droplet size,
583 fluid acoustic damping properties and SAW damping length[89]. ARF occurs when the
584 vibrational oscillations from the acoustic wave-induced a non-oscillating force on

585 particles within a fluid or an interface within fluids. ARF consists of primary forces and
586 secondary forces, where the first one causes particles to move about in an acoustic
587 field or cluster in pressure nodes or antinodes in standing waves. The secondary one,
588 however, involves particle-particle interactions which are not related to droplet sorting.
589 In most cases, it is difficult to compare and determine the influences of AS and ARF
590 separately as both are induced upon actuation. A more appropriate method of
591 categorizing the use of acoustic controls would be in the type of wave used. Droplet
592 sorting has been reported using three different types of waves, namely the travelling
593 SAW, the standing SAW and lastly the BAW.

594

595 **1. 3. 5. 1. Travelling Surface Acoustic Wave (TSAW)**

596 TSAW was demonstrated by Franke et al. [90], where a pair of electrodes was
597 fabricated beside a channel, Figure 1.17a,b. Monodispersed water droplets generated
598 entered the upper channel without activation of the SAW as the cross-section of the
599 upper channel was designed to be larger. Upon actuation of the SAW, the droplets
600 flowed towards the lower channel. Polyacrylamide (PAM) particles were also used to
601 demonstrate the sorting. This actuation was credited to acoustic streaming, based on
602 the compressibility of the continuous phase at the high frequency used for SAW
603 excitation. The frequency used here is 140MHz. Another review paper by Xi et al. [11]
604 disagreed with this statement mentioning that the κ value of the droplets used in this
605 experiment was above a critical value meaning that ARF was also induced. Here,

606 $$\kappa = \frac{\pi d}{\lambda_f} \quad (17)$$

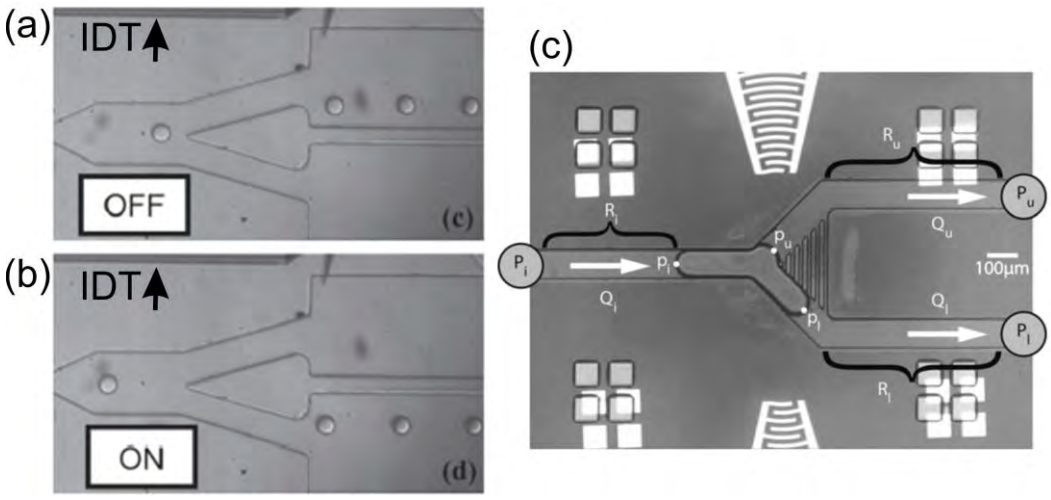

Figure 1.17. Droplet sorting using travelling surface acoustic waves (TSAW). (a-b) Before activation, the water droplets flow into the upper channel. Upon activation, the droplets flow into the lower channel[90]. (c) Image of the device using focused IDTs to steer plugs away from activated electrode[91]. Reprinted from [90, 91] with permission from the Royal Society of Chemistry, Copyright 2009, 2015.

where d refers to the particle or droplet diameter and λ_f the fluid wavelength (m) used. Their evaluation of this was based on the experimental findings by Skowronek et al.[92], which showed the influence of ARF on the particles when $\kappa > 1$. Further experiments need to be conducted to determine whether AS and/or ARF was induced. The device was subsequently improved to also enable cell sorting. However, the type of wave was converted to BAW through the presence of PDMS posts between the microfluidic channel and piezoelectric substrate[93]. A high sorting frequency of 3kHz was obtained for the sorting of cells in this device. However, droplet sorting frequency was not mentioned in the paper. Sorting was successfully demonstrated using focused IDTs at high power values on plugs as observed in Figure 1.17c[91]. The acoustic energy was used in this case to compensate for the decreasing pressure at one channel, enabling the fluid to fill up the other channel and subsequently drawing the plug in.

1. 3. 5. 2. Standing Surface Acoustic Wave (SSAW)

SSAW was generated when two IDTs were activated in opposite directions of the crystallographic plane. The interference from these two waves then forms a series of pressure nodes and antinodes. This is determined by the equation:

$$f = \frac{c}{\lambda}, \tag{18}$$

where f, c and λ are the resonant frequency, speed of sound in medium (m/s) and wavelength in medium, respectively. Spherical particles or droplets that are placed in this acoustic field would then propagate towards either the pressure nodes or antinodes depending on their acoustic contrast factor, which is given as [94]

$$\phi(\beta, \rho) = \frac{5\rho_d - 2\rho_c}{2\rho_d + \rho_c} - \frac{\beta_d}{\beta_c}, \tag{19}$$

where ρ_d, ρ_c, β_d and β_c are the density of the sphere, the density of the fluid, the compressibility of the object and compressibility of the fluid. For a positive $\phi(\beta, \rho)$, the particle would travel to a pressure node. If negative, the particle would travel to an antinode. The force experienced by the sphere would also be given as:

$$F = -\left(\frac{\pi p^2 V_o \beta_f}{2\lambda}\right) \phi(\beta, \rho) \sin(2k, x), \tag{20}$$

where p, V_o and λ are the acoustic pressure, the volume of a sphere and acoustic wavelength. These set of equations can also be used for small spherical droplets, as proven by Li et al [95]. The schematic diagram is given in Figure 1.18. In this device, single droplets could be sorted into five different channels using five different SSAW frequencies. Chirped IDTs were used in this case that were mentioned to generate larger ARF, pushing droplets faster in the perpendicular direction. These IDTs had

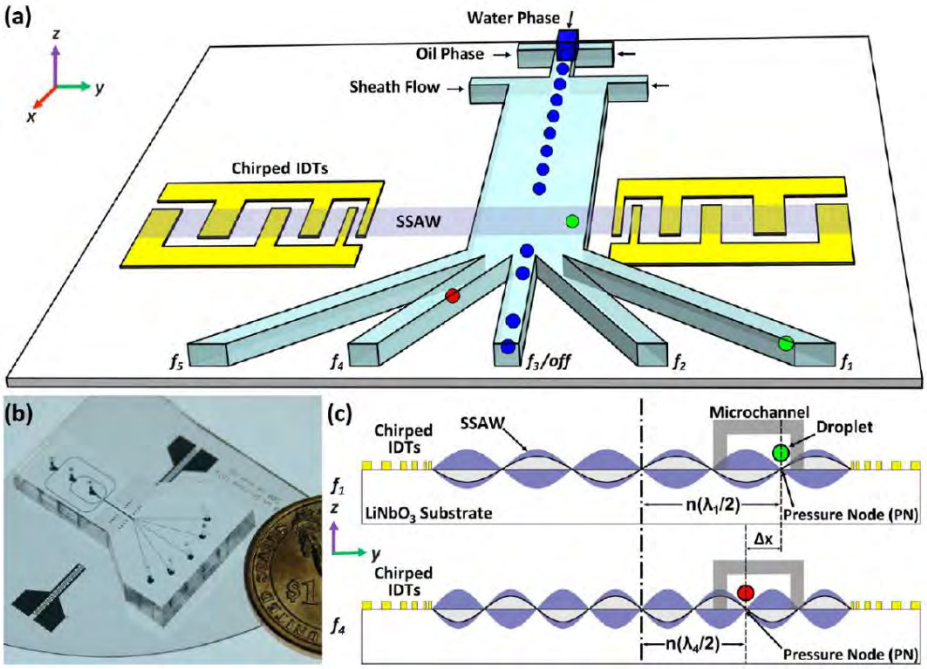

Figure 1.18. Droplet sorting using standing surface acoustic waves (SSAW). (a) Schematic diagram of the device showing the effects of SSAW on droplets of different density. Inset shows the movement of alginate droplets upon actuation of acoustic wave. (b) Photo of actual device. (c) SSAW effects on droplet sorting. Reprinted from [95] with permission from the American Chemical Society, Copyright 2013.

fingers with decreasing widths closer to the fluidic channel. However, the experiments were run only based on 40-50μm droplets, that are less than the wavelength of the frequencies used. If larger diameters were used, the equations mentioned above might not be suitable. Another device was developed by Nam et al. [96], where cell sorting was carried out at 97% accuracy rate for large cell quantity beads. In this device, sorting was based on the density of each cell-encapsulated alginate bead droplets which affected the $\phi(\beta, \rho)$ variable of the equation given above. Over 2,300 droplets were sorted per minute with acceptable cell viability.

1. 3. 5. 3. Bulk Acoustic Wave (BAW)

650 BAW is defined as the elastic wave in a solid that propagate through the bulk
651 material. Unlike SAW that travels along the surface of a material, BAWs travel within
652 a material utilising compressional waves (pressure waves) or transverse waves (shear
653 waves)[98]. Materials with high acoustic impedance are generally used to construct
654 BAW-based microfluidic devices, with common materials being silicon and glass[97, 99].
655 Because of the difference in impedance at the fluid or structural interface, the acoustic
656 energy is reflected into the fluid, resulting in a stronger acoustic field. One good
657 implementation of this was reported by Leibacher et al. [97] who dry-etched a silicon
658 wafer to produce microchannels with a sorting chamber, Figure 1.19. Using this
659 approach, the acoustic energy lost, through the substrate is minimized and droplet
660 sorting was observed when the transducer frequency was switched from 463 kHz (λ/2
661 mode) to 979 kHz (λ mode). Another interesting device using BAW was reported by
662 Phan et al. [100], who used a thin silicon nitride layer to generate acoustic forces for
663 droplet sorting. The silicon nitride layer was placed right below a sorting channel where
664 repulsion of droplets was observed when activated. Lee et al. [101] managed to sort

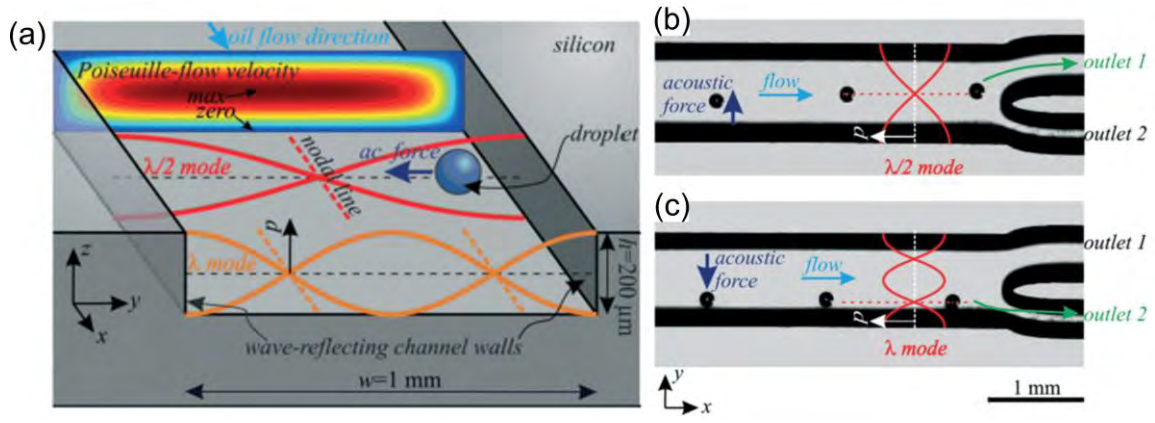

Figure 1.19. Sorting using bulk acoustic waves (BAW). (a) Schematic diagram illustrating acoustic waveforms at λ/2 mode and λ mode. (b) Sorting at λ/2 mode. (c) Sorting at λ mode. Reprinted from [97] with permission from the Royal Society of Chemistry, Copyright 2015.

100μm diameter lipid droplets in water by placing a 30 MHz transducer beside a microchannel to generate BAW. A schematic diagram of the device is shown in Figure 1.20. As the acoustic impedance of PDMS was similar to water, the transducer and the device were both submerged in a water bath for maximum transmission. Sorting was carried out when a droplet was detected by the transducer itself through backscattering of the acoustic waves. The device gave a high sorting efficiency of 99.3% for 50μm droplets and 100μm droplets.

1. 4. Active Droplet Coalescence

Active methods for droplet coalescence involve an external energy source that either affects the rate of film thinning between droplets or induces droplet interface instability. Coalescence can be considered as a 3-step process. First, the droplets come into close proximity with each other. Second, the thin film of continuous phase fluid separating both droplets will gradually be reduced. Last, a fluidic bridge between both droplets is formed due to film rupture, resulting in merging of the droplets[102]. Applications using droplet coalescence has been expanded to also allow users to carry out droplet picoinjection[103, 104]. Active methods provide the advantage of selectivity in merging, where users can target specific droplets to merge as compared to passive methods. This concept is highly suitable for applications involving simultaneous screening of different samples within a device[105, 106]. A list of reviews has been published by numerous research groups[102, 107-109], where a variety of methods are described to be thermal, acoustic, optical, pneumatic, magnetic and electric. The most common method is using electric fields[110]. In this section, we will give a brief introduction of each method with some examples.

1. 4. 1. Electric Control

The effect of electric field on droplet coalescence can be categorized into a few mechanisms as given by Eow et al.[110]: electrophoresis, dielectrophoresis and dipole coalescence. Electrophoresis occurs when a charged droplet is placed in a uniform electric field. The charge of the droplet thereby directs the droplet to move along the electric field direction[111]. With two oppositely charged droplets in the electric field, the attractive electrostatic forces induced by both charges cause the droplets to come together. This phenomenon was first documented by Link et al.[17], where the dispersed

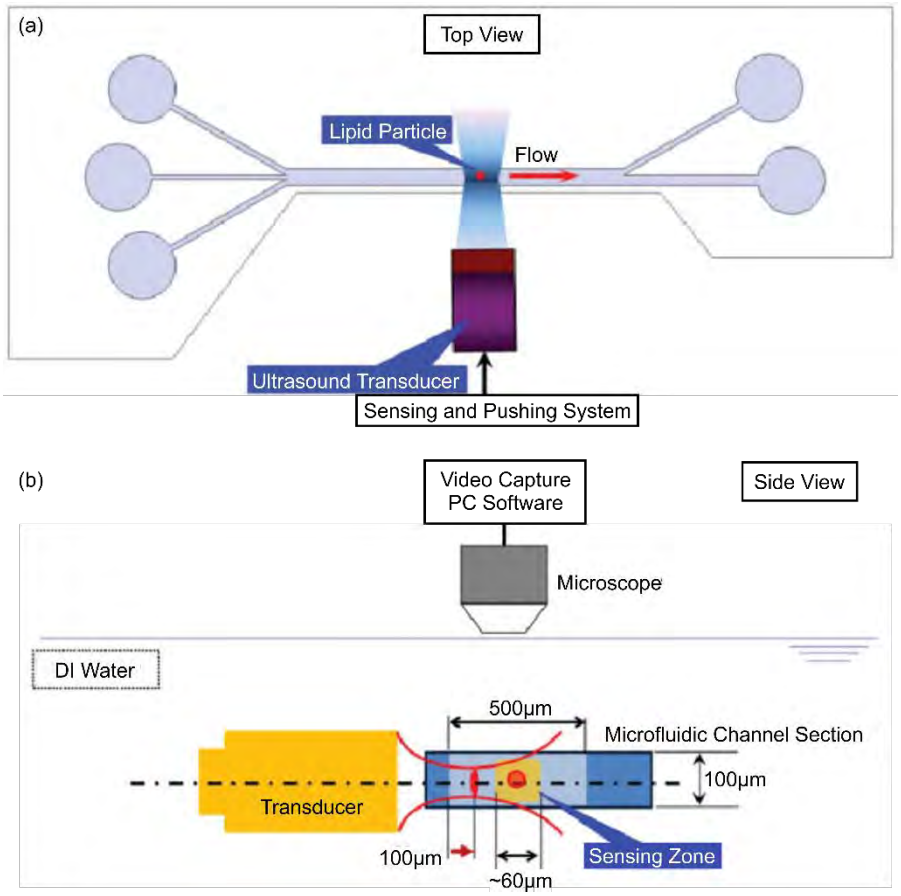

Figure 1.20. Experimental arrangement for acoustic droplet sensing and sorting device (a) Top view. (b) Side view. Reprinted from [101] with permission from the Royal Society of Chemistry, Copyright 2012.

698 phases were separately charged by direct contact with a positive and ground
699 electrode. This process resulted in the formation of droplets, which are oppositely
700 charged flow into a main channel. The synchronisation of the droplet generation
701 causes the charged droplets to be close enough for electrostatic attraction forces to
702 overcome the separation, leading to merging.

703 A more comprehensive study of this phenomenon was conducted by Priest et
704 al. [113]. The authors demonstrated the effect of charging of the aqueous phases using
705 both pulsed AC and DC electric signals on droplet coalescence. A linear relationship
706 between the applied voltage against the separation distance of the droplet interfaces
707 was established using different salt solutions. His results revealed that the
708 coalescence is attributed to the field-induced dynamic instability of the oil-water
709 interfaces, resulting in electrocoalescence. This phenomenon is similar to the
710 observation made by Niu et al. [114]. Similar experiments were also carried out by Liu et

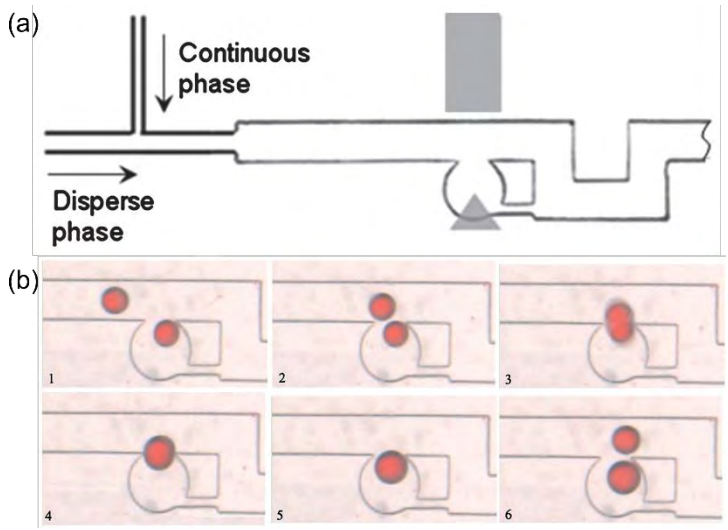

Figure 1.21. Electrocoalescence using dielectrophoretic forces together with droplet traps. (a) Electrodes are placed underneath the channel as given in the grey blocks. (b) Sequential images of merging droplets as observed under a microscope. Reprinted from [112] with permission from the Royal Society of Chemistry, Copyright 2009.

al.[115], who further discussed the influence of surfactants within the system. The concentration of the surfactant was observed to result in a higher critical voltage for merging[115] because the surfactant molecules are electrically charged themselves[116]. As a result, the electric field affects both droplet and surfactant molecules. Surfactant molecules redistribute and realign based on the concentration and electric field properties.

Dielectrophoresis (DEP) in droplet coalescence is similar to droplet sorting, where uncharged droplets move towards regions of higher electric field due to

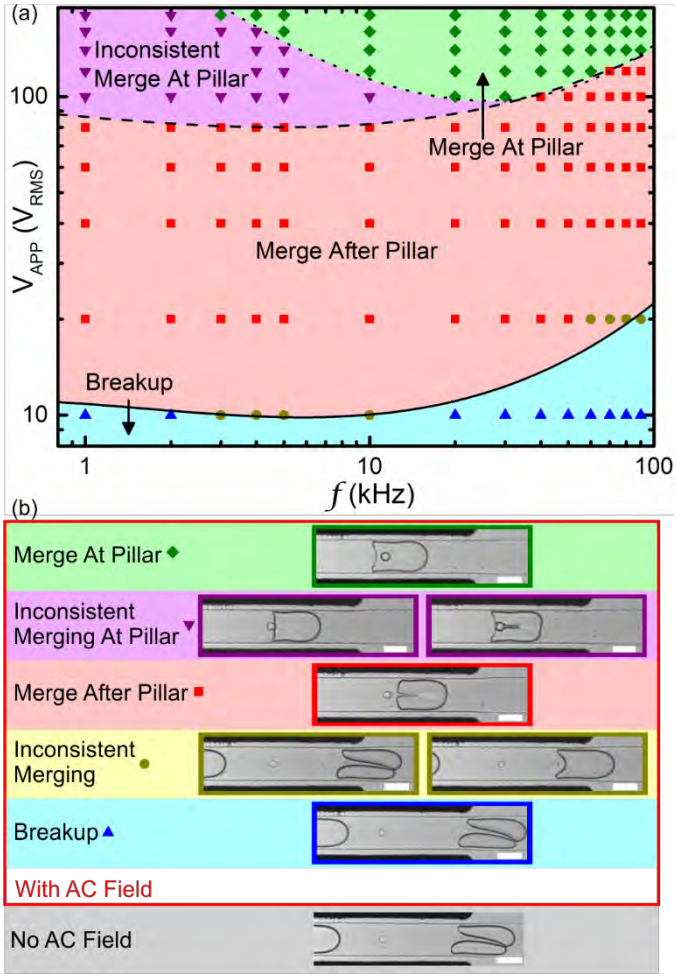

Figure 1.22. On-demand droplet electrocoalescence showing different coalescence regimes based on applied voltage V_{APP} and AC frequency f. Reprinted from [117] with permission from the American Chemical Society, Copyright 2019.

polarization. As the electric field used is non-uniform, one end of the dipole is stronger than the other, thereby causing the force. One use of DEP force in electrocoalescence is with the combination of a droplet trap as demonstrated by Wang et al. [112] as shown in Figure 1.21. The DC signal pushes the droplets into a microwell where subsequent merging can take place. However, the merging phenomenon was not clearly described in this paper. Upon the activation of the electric field, the polarization of the droplets results in a dipole-dipole interaction between the two droplets[118]. Coalescence was thus obtained due to the instability of the thin film between the two droplets.

Dipole coalescence was mentioned to be an extension of this DEP as the droplet dipoles themselves induce an electric field, adding on to the attraction force[110]. Lee et al.[119] demonstrated this using a 1kV DC signal passing through electrodes at the droplet merging junction. This junction also acts as a trap that holds the droplets in place before merging. Likewise, this method was also modified to enable serial dilution using AC electric signals[120]. By enabling coalescence across the interface of the two droplets, fluid from the concentrated droplet can be mixed with the moving droplet. Multiple droplet sizes were also observed to be generated using on-demand droplet coalescence across a micropillar through this mechanism, Figure 1.22[117].

1. 4. 2. Magnetic Control

738 Magnetic controls in droplet coalescence are mainly based on the type of
739 magnetic field used. For non-uniform magnetic fields, droplets are attracted by the field
740 and trapped. Ray et al. [121] demonstrated this entrapment as shown in Figure 1.23a.
741 Initial Ferrofluid Droplets (IFD) were trapped by the presence of a permanent magnet
742 alongside the fluidic channels. The trapped droplets coalesce to form a large
743 Coalesced Ferrofluid Droplet (CFD) under the presence of the non-uniform magnetic
744 field. Subsequently, the influence of flow rate, fluid viscosity and magnetic field

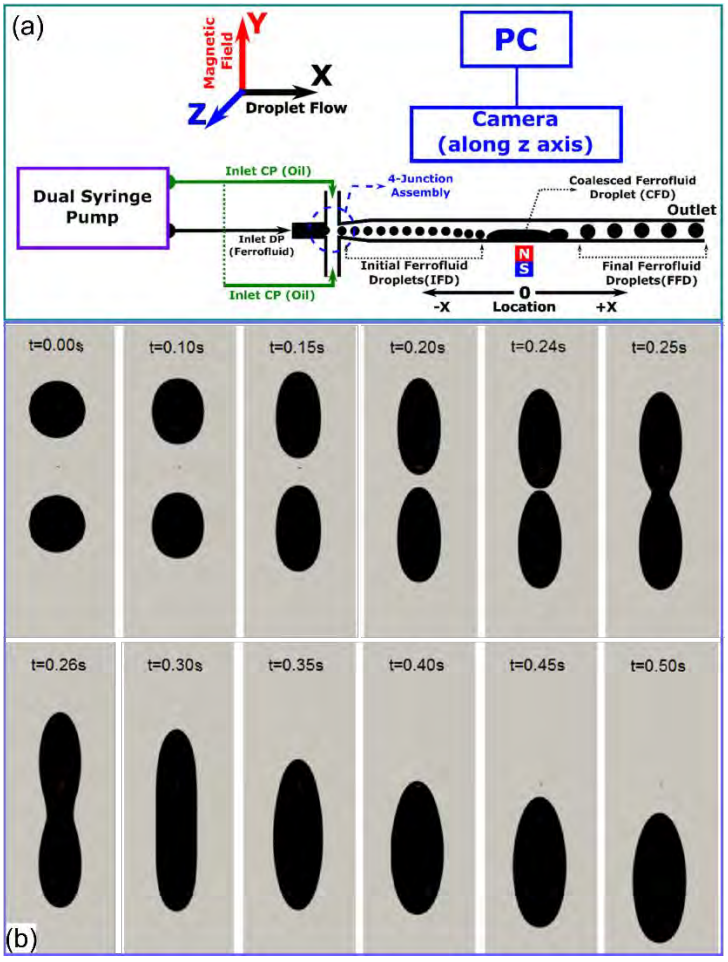

Figure 1.23. (a) Experimental setup for non-uniform magnetic field induced droplet merging[121]. A paramagnet is placed on one side of the fluidic channel as depicted. (b) Droplets in a uniform magnetic field along the same direction as flow showing induced merging at different time points during experiment[122]. Reprinted and adapted from [121, 122] by permission from Elsevier, Copyright 2017, 2015.

strength causes the release of droplets from the CFD volume downstream. This consequently results in the generation of the Final Ferrofluid Droplets (FFD) with volume control. Size of the FFD, however, is difficult to predict due to the non-linearity across different constituent forces, namely the inertial, pressure-induced, viscous and magnetic forces. Apart from single emulsion droplets, the coalescence of double emulsion droplets was also demonstrated using this trapping phenomenon[123]. Due to the non-uniform magnetic field, the paramagnetic ionic liquid (MIL) at the core of the double emulsion is attracted to the magnet used. This traps the emulsion until a subsequent emulsion collides with it, merging both droplets. The release of the large droplet was then carried out by the removal of the magnet from the side of the fluidic channel. Using this same concept, merging between an emulsion with and without a MIL core was also demonstrated using NdFeB magnets.

Ferrofluid droplets were observed to undergo deformation in the presence of a uniform magnetic field across the fluidic channel[124]. Under the induced magnetic forces, the ferrofluid droplets elongate along the direction of the magnetic field. The final shape of the droplet is determined by a balance of the magnetic force and the interfacial tension of the droplet. Simulations and experimental studies carried out by Ghaffari et al [122] revealed that although under a uniform magnetic field, the regions of the highest magnetic stress are at the poles of the droplet. This results in an increased curvature of the droplet at the poles and decreased at the midsection. Accordingly, with the flow direction and electric field in parallel with each other, the elongation of two separated droplets eventually resulted in merging. It was also observed that the magnetic volume force that acts on a droplet affects the interfacial tension, leading to the deformation of the droplet[125]. This phenomenon is depicted in Figure 1.23b. This force is influenced by the concentration of magnetic particles, magnetic susceptibility

and droplet volume, accordingly affecting droplet actuation and merging[126]. Droplet trapping under a uniform magnetic field can be used for droplet coalescence[127]. Using a low flow rate and a strong magnetic force, a droplet can be trapped in a microchannel until a subsequent droplet collided with it[127]. Upon merging, the kinetic energy of the second droplet and the increased viscous force of the new droplet caused the release of the droplet from the magnetic field.

1. 4. 3. Thermal Control

Thermal controls in droplet coalescence are similar in concept to the ones used in droplet sorting. Likewise, both resistive heating and localized heating using lasers are employed for coalescence. In resistive heating, the high temperature reduces the viscosity and interfacial tension of the fluid, inherently increasing fluid velocity. When applied on a bypass channel as given in Figure 1.24[128], the flow of the continuous phase through the bypass channel increases. This process causes the two

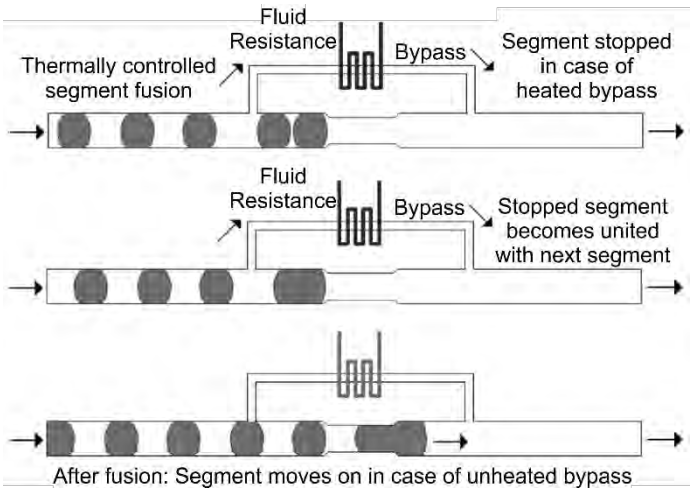

Figure 1.24. Droplet coalescence induced through resistive heating on bypass channel. Reprinted and adapted from [128] by permission from Elsevier, Copyright 2004.

droplets to come into close proximity at the main channel. Subsequent drag forces induce merging and finally push the droplet through the confined segment. When heating is applied on the expansion channel, the heat reduces the viscosity of the continuous phase while increasing the interfacial tension of the droplet. This firstly causes the continuous phase to flow out of the chamber faster, while the droplet reduces in velocity due to the expansion. With a subsequent droplet entering the expansion chamber, merging would then occur. For droplets that are larger than the expansion channel itself, the temperature difference at the outlet of the chamber also plays a part. The lower temperature outside the chamber reduces the interfacial tension, inducing a resistance to droplet flow and allowing the second droplet to enter the expansion chamber. Thermocapillary force pushes both droplets together and cause merging[129]. However, droplets that are smaller than the expansion channel requires a minimum critical temperature for merging to happen[130].

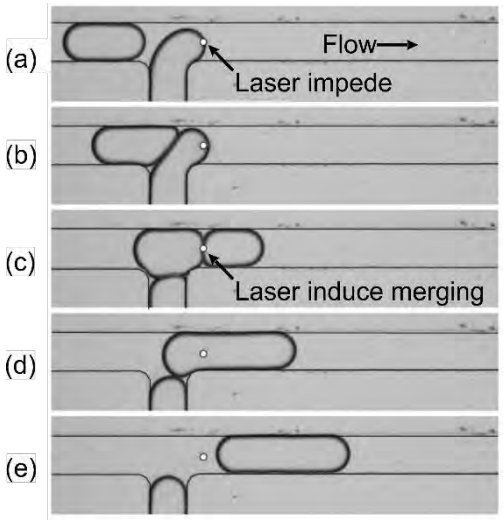

Figure 1.25. Localized heating induced droplet coalescence, where (a-e) shows different stages of droplet motion and merging[131]. Reprinted and adapted from [131] by permission from the Royal Society of Chemistry, Copyright 2007.

Localised heating using lasers has also been observed to induce droplet coalescence. Coalescence happens through either the redistribution of surfactant molecules[131] or the decrease in interfacial tension at the laser spot[71]. The laser spot causes the droplet to have a Marangoni effect[132] stopping its motion while at the same time also affect the viscosity of the fluid at the laser spot. Baroud et al. [131] make use of these two attributes to induce merging by first trapping one fluid interface at the laser spot until a second droplet collides with it upstream. This pushes the first fluid interface to form a droplet and move past the laser spot until the laser point is at the droplet-droplet interface, where the droplets merge subsequently. This phenomenon is shown in Figure 1.25. Another demonstration of this localised heating was done by Fradet et al. [71], who used wells to trap the two droplets of different media before laser activation. This method displays high selectivity for activation, making it a useful platform for array-based biological experiments.

1. 4. 4. Pneumatic Control

Pneumatic controls for droplet coalescence require microvalves as the droplets have to be trapped first before merging can take place. The microvalves for this purpose are also similar to the ones mentioned for droplet sorting where they are either on the side of the microchannels[85, 86] or directly on top of it[84]. The former is used in conjunction with micropillar arrays that trap the droplets in their position due to the interfacial tension against the micropillars. The microvalves control the flow rate across the main channel or bypass channel as given in Figure 1.26a through adjustment of their respective channel widths[133]. This accordingly affects the droplet trapping time within the micropillar array which subsequently controls the number of droplets merged

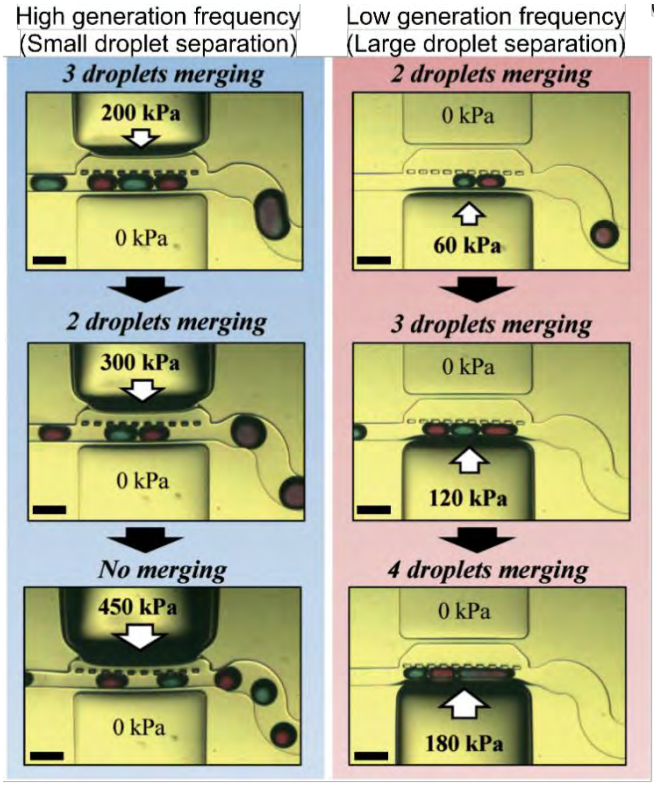

Figure 1.26. Droplet merging controlled by pneumatic actuation of side microvalves[133]. Reprinted from [133] by permission from the Royal Society of Chemistry, Copyright 2014.

821 in the process. Without pneumatic actuation, passive merging is still attainable, when
822 the bypass channel is blocked by the accumulated droplets[134]. The number of droplets
823 to be merged however would not be controllable. The application of this technique has
824 been used for copper complex synthesis[133].

825 Another technique using this same concept of trapping droplets is demonstrated using
826 the so-called Quake's valves. However, this valve is placed directly over a main fluidic
827 channel, stopping droplets upon actuation. This allows a subsequent droplet to collide
828 into the trapped droplet and merge over time before the valve is deactivated to release
829 the merged droplet[50]. Figure 1.26b shows the merging phenomenon. Multiple Quake's
830 valves were also integrated into a system to enable single droplet merging[135]. By
831 sequentially activating different pneumatic actuators, Guo et al. [135] was able to

demonstrate trapping and subsequent merging which was almost similar to picoinjection[136].

1. 4. 5. Acoustic Control

Droplet coalescence has been demonstrated using both surface acoustic waves and bulk acoustic waves. Using arc-shaped interdigitated transducers, focused surface acoustic waves are generated to hold the droplet in its position within an expansion chamber[137]. The subsequent droplet then collides with it and merges, causing the droplet to break away from the trap due to drag forces, Figure 1.27a. This trapping process of droplets with diameters similar to the wavelength of the acoustic wave occurs as such droplets are attracted towards the high-intensity zones within an acoustic field. By increasing the acoustic power, the droplet remains trapped for a longer period enabling multiple droplets to coalesce before being released.

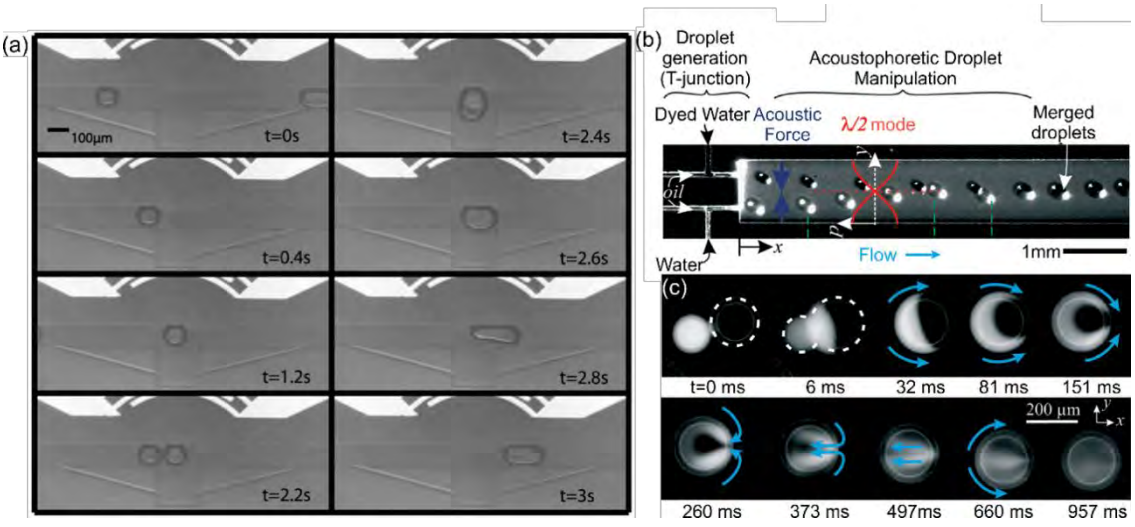

Figure 1.27. Droplet coalescence using (a) focused surface acoustic waves[137] and (b) bulk acoustic waves[97]. Reprinted and adapted from [97, 137] by permission from the Royal Society of Chemistry, Copyright 2014, 2015.

Accordingly, the system has demonstrated merging of up to 4 droplets consecutively where each droplet diameter is approximately 80 μm, similar to electrode wavelength.

Bulk acoustic waves have been used for droplet coalescence, where the acoustic force generated pushes droplets from two different sources together into a centreline[97]. A similar phenomenon was demonstrated in droplet sorting. Leibacher et al.[97] hypothesized that the merging phenomenon was caused by both hydrodynamic effects and secondary acoustic forces that arise from the bulk acoustic wave. This phenomenon was however not studied extensively. Nevertheless, fluorescence tests also reveal that the merged droplets proved complete mixing as shown in Figure 1.27b. One main disadvantage, however, is that synchronisation of the two droplets have to be carried out first before merging can take place. The distance between each aligned droplet has to be adjusted and optimized for merging.

1. 4. 6. Optical Control

Optical controls in droplet coalescence had been demonstrated through the use of lasers or photosensitive surfactants. Lasers were observed to have both thermal and optical effects on droplets. The thermal aspects have already been covered above. Therefore, the optical aspect would be discussed here. An optical gradient force is produced when a droplet enters the focal volume of a laser beam due to the change in the photon momentum across the optical interface[138]. This is determined by the difference in refractive index across the two different media, pulling the droplet towards the centre of the laser axis. This optical force, therefore, acts as a trapping mechanism that holds the droplet in its position. The laser intensity required for this depends on a few criteria such as the size of the beam waist, the droplet velocity, the

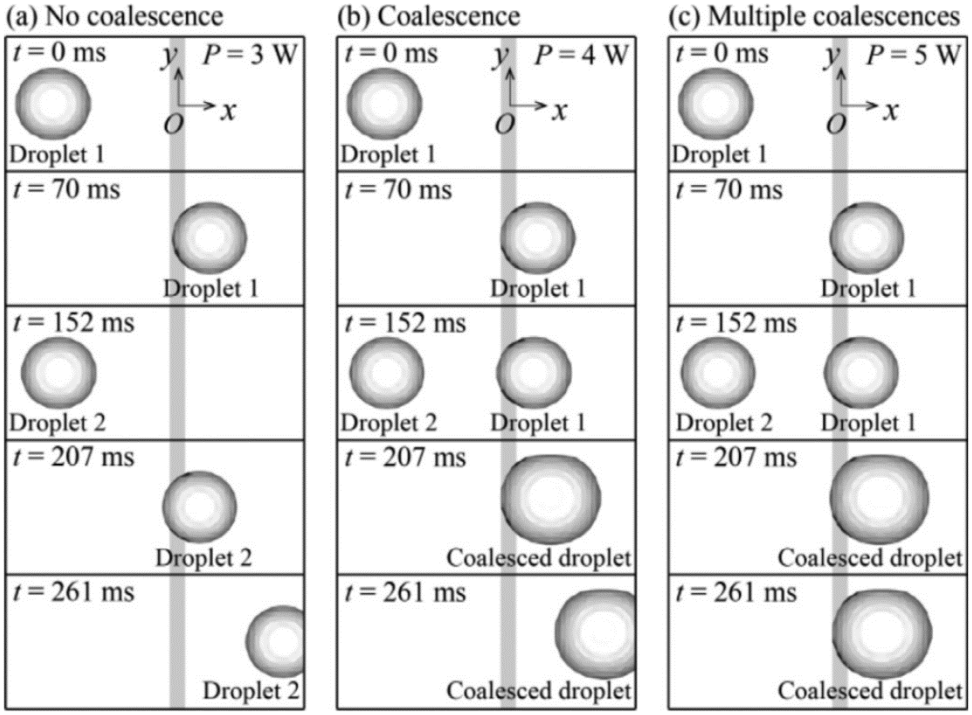

Figure 1.28. Merging using optical gradient force with (a-c) showing the snapshots of different laser beam powers. Multiple coalescences are also observed at higher laser beam powers Reprinted from [139] by permission from Elsevier, Copyright 2015.

droplet size, the medium viscosity and the refractive indices[139]. Based on these values, the number of droplets merging can also be controlled. A merging regime diagram has been developed by Jung et al.[140] as shown in Figure 1.28.

The exposure of fluids mixed with photosensitive surfactant also enables droplet coalescence. The effect is permanent even after illumination as the chemical structure of the surfactant is modified. It is also highly dependent on the type of surfactant used. Nurdin et al. [141] made use of AzoTAB mixed in water with pure oleic acid as a continuous phase. The fluid was accordingly illuminated at the droplet generation junction in Figure 1.29a using a light-emitting diode at 365-nm wavelength. By having droplets to pass through a series of expansion chambers as given in Figure 1.29b, the chambers induced merging between the droplets. Without illumination,

instead of droplets being formed, two parallel flowing streams were instead observed from the two droplet generation junctions. The AzoTAB surfactant in the water undergoes a trans-cis isomerization under illumination that increases the interfacial energy of the water, inducing fragmentation[142]. Another type of surfactant used is mixed into the carrier oil phase with a perfluoro-polyether (PFPE) hydrophobic chain linked to a PEG-600 hydrophilic chain[143]. Using this surfactant, photolysis occurs upon illumination resulting in an increased interfacial tension of the droplet. This increasing interfacial tension accordingly attracts more surfactant molecules from the bulk medium or neighbouring droplet. With more surfactant molecules being photolysed beyond a critical level, destabilisation occurs at the interface, inducing coalescence. The time required for coalescence can also be approximated by the concentration of

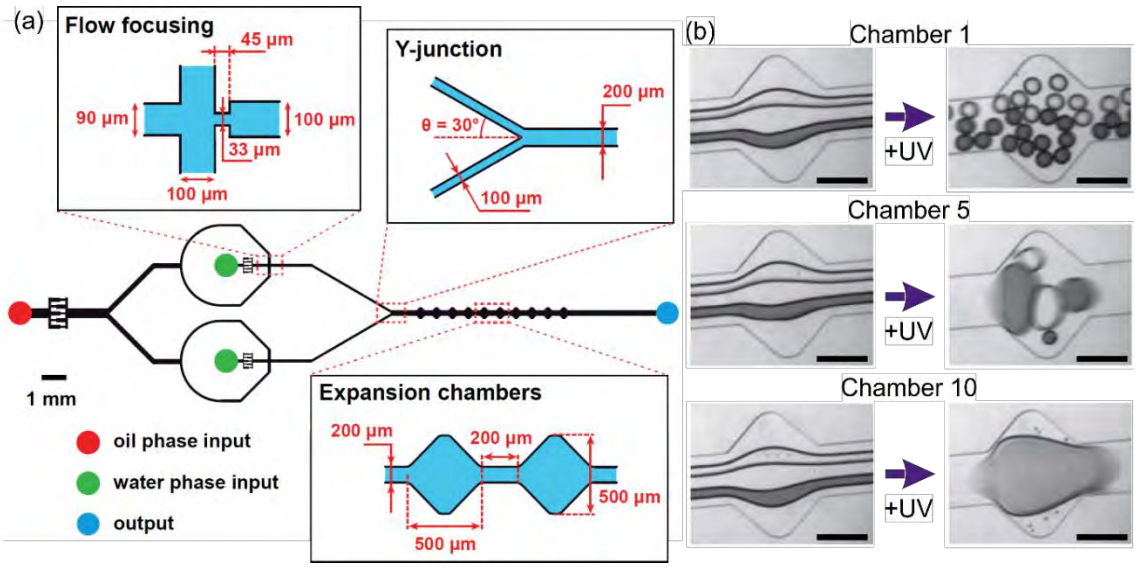

Figure 1.29. Use of photosensitive surfactant AzoTAB in water showing merging at expansion chambers. (a) Schematic diagram of the device showing two flow-focusing junctions for droplet generation where illumination occurs. (b) Images of different chambers where UV illumination causes droplets to be formed. Expansion chambers cause reduction of droplet velocities, resulting in coalescence. Scale bar represents 200µm. Reprinted and adapted from [141] with permission from Elsevier, Open Access.

surfactant, size and distance between droplets, pulse rate and size of laser beam area[143]. Accordingly, controllable and stable dual jet and dual droplet regimes are observed here which can be easily implemented for parallel high throughput screening applications.

1. 5. Conclusion

If one would consider the droplet as a tool for multidisciplinary studies, the manipulation of droplets would therefore be the key to successful implementation. Droplet generation, sorting and coalescence are accordingly three recurrent manipulations required for most reactions to occur. A repertoire of different technologies has also been developed for each manipulation as mentioned in this chapter. As each has its own sets of strengths and limitations, a fair comparison of each mechanism would be impossible. As such, this chapter here is targeted at demonstrating the variety of techniques developed for each individual manipulation. With the plethora of techniques, users are then able to evaluate and select the method that would suit their needs the most. Through considering additional factors like the availability of equipment, users can accordingly select the type of control to suit their needs.

The development of different technologies in microfluidics has also allowed more selectivity and specificity in experiments, further reducing the need for precious materials. This goes in line with the current trend for reducing resource costs amidst the global carbon-free push. Precious resources like polymer-based materials and rare media containing circulating tumour cells (CTCs) are therefore fully utilised with minimal loss. Droplet sorting also helps to alleviate this by only conducting further treatments on target droplets. Active droplet generation accordingly reduces the

amount of reagents used. Studies into droplet coalescence also provide deeper insights into the merging mechanisms to allow higher efficiency in droplet-droplet interactions. These techniques would enable the use of droplets as microreactors for experimental studies. Where each microreactor would be fully optimised to ensure the highest efficacy. With a careful selection of the type of technique, it is also believed that all laboratories would be able to conduct high-quality research exhibiting a high degree of controllability in experiments. Accordingly, this also reduces the carbon footprint of laboratories, making experiments more environmentally friendly and less costly. Finally boosting the pursuance of science without the destruction of the Earth.

1. 6. References

1. G. M. Whitesides, *Nature*, 2006, **442**, 368.
2. M. T. Guo, A. Rotem, J. A. Heyman and D. A. Weitz, *Lab on a Chip*, 2012, **12**, 2146-2155.
3. J. F. Edd, D. Di Carlo, K. J. Humphry, S. Köster, D. Irimia, D. A. Weitz and M. Toner, *Lab on a Chip*, 2008, **8**, 1262-1264.
4. A. Huebner, D. Bratton, G. Whyte, M. Yang, A. J. deMello, C. Abell and F. Hollfelder, *Lab on a Chip*, 2009, **9**, 692-698.
5. P. Li, Z. Ma, Y. Zhou, D. J. Collins, Z. Wang and Y. Ai, *Analytical Chemistry*, 2019.
6. A. R. Abate, T. Hung, R. A. Sperling, P. Mary, A. Rotem, J. J. Agresti, M. A. Weiner and D. A. Weitz, *Lab on a Chip*, 2013, **13**, 4864-4869.
7. X. Niu, S. Gulati and J. B. Edel, *Lab on a chip*, 2008, **8**, 1837-1841.
8. D. Link, S. L. Anna, D. Weitz and H. Stone, *Physical review letters*, 2004, **92**, 054503.
9. S. H. Tan, F. Maes, B. Semin, J. Vrignon and J.-C. Baret, *Scientific Reports*, 2014, **4**, 4787.
10. J.-C. Galas, D. Bartolo and V. Studer, *New Journal of Physics*, 2009, **11**, 075027.
11. H.-D. Xi, H. Zheng, W. Guo, A. M. Ganan-Calvo, Y. Ai, C.-W. Tsao, J. Zhou, W. Li, Y. Huang, N.-T. Nguyen and S. H. Tan, *Lab on a Chip*, 2017, **17**, 751-771.
12. P. Zhu and L. Wang, *Lab on a Chip*, 2017.
13. D. J. Eastburn, A. Sciambi and A. R. Abate, *Plos One*, 2013, **8**, e62961.
14. B. O'Donovan, D. J. Eastburn and A. R. Abate, *Lab on a Chip*, 2012, **12**, 4029-4032.
15. B. O'Donovan, T. Tran, A. Sciambi and A. Abate, *Journal of visualized experiments: JoVE*, 2014.
16. Z. Z. Chong, S. H. Tan, A. M. Gañán-Calvo, S. B. Tor, N. H. Loh and N.-T. Nguyen, *Lab on a Chip*, 2016, **16**, 35-58.
17. D. R. Link, E. Grasland-Mongrain, A. Duri, F. Sarrazin, Z. Cheng, G. Cristobal, M. Marquez and D. A. Weitz, *Angewandte Chemie International Edition*, 2006, **45**, 2556-2560.
18. H. Gu, C. U. Murade, M. H. Duits and F. Mugele, *Biomicrofluidics*, 2011, **5**, 011101.
19. A. M. Gañán-Calvo, W. Guo, H.-D. Xi, A. J. T. Teo, N.-T. Nguyen and S. H. Tan, *Physical Review E*, 2018, **98**, 032602.

20. W. Guo, A. J. T. Teo, A. M. Gañán-Calvo, C. Song, N.-T. Nguyen, H.-D. Xi and S. H. Tan, *Physical Review Applied*, 2018, **10**, 054045.
21. M. He, J. S. Kuo and D. T. Chiu, *Langmuir*, 2006, **22**, 6408-6413.
22. S. Hardt and F. Schönfeld, *Microfluidic technologies for miniaturized analysis systems*, Springer Science & Business Media, 2007.
23. P. He, H. Kim, D. Luo, M. Marquez and Z. Cheng, *Applied Physics Letters*, 2010, **96**, 174103.
24. Y. Wu, T. Fu, Y. Ma and H. Z. Li, *Soft Matter*, 2013, **9**, 9792-9798.
25. N. Pamme, *Lab on a Chip*, 2006, **6**, 24-38.
26. T. Say-Hwa, N. Nam-Trung, Y. Levent and K. Tae Goo, *Journal of Micromechanics and Microengineering*, 2010, **20**, 045004.
27. S. H. Tan and N.-T. Nguyen, *Physical Review E*, 2011, **84**, 036317.
28. J. Liu, Y. F. Yap and N.-T. Nguyen, *Physics of Fluids*, 2011, **23**, 072008.
29. J. Liu, S.-H. Tan, Y. F. Yap, M. Y. Ng and N.-T. Nguyen, *Microfluidics and Nanofluidics*, 2011, **11**, 177-187.
30. N.-T. Nguyen, T.-H. Ting, Y.-F. Yap, T.-N. Wong, J. C.-K. Chai, W.-L. Ong, J. Zhou, S.-H. Tan and L. Yobas, *Applied Physics Letters*, 2007, **91**, 084102.
31. C. A. Stan, S. K. Tang and G. M. Whitesides, *Analytical chemistry*, 2009, **81**, 2399-2402.
32. S. S. Murshed, S. H. Tan, N. T. Nguyen, T. N. Wong and L. Yobas, *Microfluidics and nanofluidics*, 2009, **6**, 253-259.
33. S. S. Murshed, S.-H. Tan and N.-T. Nguyen, *Journal of Physics D: Applied Physics*, 2008, **41**, 085502.
34. C.-H. Yeh, K.-R. Chen and Y.-C. Lin, *Microfluidics and nanofluidics*, 2013, **15**, 775-784.
35. V. Miralles, A. Huerre, H. Williams, B. Fournie and M.-C. Jullien, *Lab on a Chip*, 2015, **15**, 2133-2139.
36. C. N. Baroud, J.-P. Delville, F. Gallaire and R. Wunenburger, *Physical Review E*, 2007, **75**, 046302.
37. A. J. T. Teo, K.-H. H. Li, N.-T. Nguyen, W. Guo, N. Heere, H.-D. Xi, C.-W. Tsao, W. Li and S. H. Tan, *Analytical Chemistry*, 2017.
38. M. E. Dolega, S. Jakiela, M. Razew, A. Rakszewska, O. Cybulski and P. Garstecki, *Lab on a Chip*, 2012, **12**, 4022-4025.
39. H. Zhou and S. Yao, *Microfluidics and Nanofluidics*, 2014, **16**, 667-675.
40. S. Zeng, B. Li, X. o. Su, J. Qin and B. Lin, *Lab on a Chip*, 2009, **9**, 1340-1343.
41. A. Raj, R. Halder, P. Sajeesh and A. Sen, *Microfluidics and Nanofluidics*, 2016, **20**, 102.
42. S. Jakiela, P. R. Debski, B. Dabrowski and P. Garstecki, *Micromachines*, 2014, **5**, 1002-1011.
43. J.-H. Wang and G.-B. Lee, *Micromachines*, 2013, **4**, 306-320.
44. C.-Y. Lee, Y.-H. Lin and G.-B. Lee, *Microfluidics and nanofluidics*, 2009, **6**, 599-610.
45. S.-K. Hsiung, C.-T. Chen and G.-B. Lee, *Journal of Micromechanics and Microengineering*, 2006, **16**, 2403.
46. S.-Y. Jung, S. T. Retterer and C. P. Collier, *Lab on a Chip*, 2010, **10**, 2688-2694.
47. H. Willaime, V. Barbier, L. Kloul, S. Maine and P. Tabeling, *Physical review letters*, 2006, **96**, 054501.
48. A. R. Abate, M. B. Romanowsky, J. J. Agresti and D. A. Weitz, *Applied Physics Letters*, 2009, **94**, 023503.
49. H.-W. Wu, Y.-C. Huang, C.-L. Wu and G.-B. Lee, *Microfluidics and nanofluidics*, 2009, **7**, 45-56.
50. B.-C. Lin and Y.-C. Su, *Journal of Micromechanics and Microengineering*, 2008, **18**, 115005.
51. J. Xu and D. Attinger, *Journal of Micromechanics and Microengineering*, 2008, **18**, 065020.
52. Y. N. Cheung and H. Qiu, *Journal of micromechanics and microengineering*, 2012, **22**, 125003.
53. Y. N. Cheung and H. Qiu, *Physical Review E*, 2011, **84**, 066310.
54. L. Schmid and T. Franke, *Lab on a Chip*, 2013, **13**, 1691-1694.
55. L. Schmid and T. Franke, *Applied Physics Letters*, 2014, **104**, 133501.

56. D. J. Collins, T. Alan, K. Helmerson and A. Neild, *Lab on a Chip*, 2013, **13**, 3225-3231.
57. Z. Ma, A. J. T. Teo, S. H. Tan, Y. Ai and N.-T. Nguyen, *Micromachines*, 2016, **7**, 216.
58. S. Yan, S. H. Tan, Y. Li, S. Tang, A. J. T. Teo, J. Zhang, Q. Zhao, D. Yuan, R. Sluyter, N. T. Nguyen and W. Li, *Microfluidics and Nanofluidics*, 2017, **22**, 8.
59. J.-C. Baret, O. J. Miller, V. Taly, M. Ryckelynck, A. El-Harrak, L. Frenz, C. Rick, M. L. Samuels, J. B. Hutchison and J. J. Agresti, *Lab on a Chip*, 2009, **9**, 1850-1858.
60. A. C. Hatch, A. Patel, N. R. Beer and A. P. Lee, *Lab on a Chip*, 2013, **13**, 1308-1315.
61. M. G. Simon and A. P. Lee, in *Microdroplet Technology*, Springer, 2012, pp. 23-50.
62. A. Sciambi and A. R. Abate, *Lab on a Chip*, 2015, **15**, 47-51.
63. A. Sciambi and A. R. Abate, *Lab on a Chip*, 2014, **14**, 2605-2609.
64. K. Ahn, C. Kerbage, T. P. Hunt, R. Westervelt, D. R. Link and D. Weitz, *Applied Physics Letters*, 2006, **88**, 024104.
65. B. Ahn, K. Lee, R. Panchapakesan and K. W. Oh, *Biomicrofluidics*, 2011, **5**, 024113.
66. B. Ahn, K. Lee, R. Louge and K. W. Oh, *Biomicrofluidics*, 2009, **3**, 044102.
67. R. Pethig, *Biomicrofluidics*, 2010, **4**, 022811.
68. C. Alexiou, W. Arnold, R. J. Klein, F. G. Parak, P. Hulin, C. Bergemann, W. Erhardt, S. Wagenpfeil and A. S. Luebbe, *Cancer research*, 2000, **60**, 6641-6648.
69. B. Teste, N. Jamond, D. Ferraro, J.-L. Viovy and L. Malaquin, *Microfluidics and Nanofluidics*, 2015, **19**, 141-153.
70. K. Zhang, Q. Liang, S. Ma, X. Mu, P. Hu, Y. Wang and G. Luo, *Lab on a Chip*, 2009, **9**, 2992-2999.
71. E. Fradet, C. Mcdougall, P. Abbyad, R. Dangla, D. Mcgloin and C. N. Baroud, *Lab on a Chip*, 2011, **11**, 4228-4234.
72. J. Won, W. Lee and S. Song, *Scientific Reports*, 2017, **7**, 3062.
73. A. Cazabat, F. Heslot, S. Troian and P. Carles, *Nature*, 1990, **346**, 824.
74. Y.-F. Yap, S.-H. Tan, N.-T. Nguyen, S. S. Murshed, T.-N. Wong and L. Yobas, *Journal of Physics D: Applied Physics*, 2009, **42**, 065503.
75. M. L. Cordero, D. R. Burnham, C. N. Baroud and D. McGloin, *Applied Physics Letters*, 2008, **93**, 034107.
76. S. Rybalko, N. Magome and K. Yoshikawa, *Physical Review E*, 2004, **70**, 046301.
77. C. N. Baroud, M. Robert de Saint Vincent and J.-P. Delville, *Lab on a Chip*, 2007, **7**, 1029-1033.
78. M. Robert de Saint Vincent, R. Wunenburger and J.-P. Delville, *Applied Physics Letters*, 2008, **92**, 154105.
79. Z. Cao, F. Chen, N. Bao, H. He, P. Xu, S. Jana, S. Jung, H. Lian and C. Lu, *Lab on a Chip*, 2013, **13**, 171-178.
80. J. Shemesh, A. Bransky, M. Khoury and S. Levenberg, *Biomedical Microdevices*, 2010, **12**, 907-914.
81. G. Aubry, M. Zhan and H. Lu, *Lab on a Chip*, 2015, **15**, 1424-1431.
82. Q. Zhang, P. Zhang, Y. Su, C. Mou, T. Zhou, M. Yang, J. Xu and B. Ma, *Lab on a Chip*, 2014, **14**, 4599-4603.
83. L. Wu, P. Chen, Y. Dong, X. Feng and B.-F. Liu, *Biomedical microdevices*, 2013, **15**, 553-560.
84. Y. Chen, Y. Tian, Z. Xu, X. Wang, S. Yu and L. Dong, *Applied Physics Letters*, 2016, **109**, 143510.
85. A. Abate and D. Weitz, *Applied Physics Letters*, 2008, **92**, 243509.
86. D. H. Yoon, D. Wakui, A. Nakahara, T. Sekiguchi and S. Shoji, *RSC Advances*, 2015, **5**, 2070-2074.
87. D. H. Yoon, J. Ito, T. Sekiguchi and S. Shoji, *Micromachines*, 2013, **4**, 197-205.
88. A. R. Abate, J. J. Agresti and D. A. Weitz, *Applied Physics Letters*, 2010, **96**, 203509.
89. R. J. Shilton, M. Travagliati, F. Beltram and M. Cecchini, *Advanced Materials*, 2014, **26**, 4941-4946.

90. T. Franke, A. R. Abate, D. A. Weitz and A. Wixforth, *Lab on a Chip*, 2009, **9**, 2625-2627.
91. M. Sesen, T. Alan and A. Neild, *Lab on a Chip*, 2015, **15**, 3030-3038.
92. V. Skowronek, R. W. Rambach, L. Schmid, K. Haase and T. Franke, *Analytical chemistry*, 2013, **85**, 9955-9959.
93. L. Schmid, D. A. Weitz and T. Franke, *Lab on a Chip*, 2014, **14**, 3710-3718.
94. K. Yosioka and Y. Kawasima, *Acta Acustica united with Acustica*, 1955, **5**, 167-173.
95. S. Li, X. Ding, F. Guo, Y. Chen, M. I. Lapsley, S.-C. S. Lin, L. Wang, J. P. McCoy, C. E. Cameron and T. J. Huang, *Analytical chemistry*, 2013, **85**, 5468-5474.
96. J. Nam, H. Lim, C. Kim, J. Yoon Kang and S. Shin, *Biomicrofluidics*, 2012, **6**, 024120.
97. I. Leibacher, P. Reichert and J. Dual, *Lab on a Chip*, 2015, **15**, 2896-2905.
98. K.-y. Hashimoto, in *Surface Acoustic Wave Devices in Telecommunications: Modelling and Simulation*, Springer Berlin Heidelberg, Berlin, Heidelberg, 2000, pp. 1-23.
99. L. Johansson, F. Nikolajeff, S. Johansson and S. Thorslund, *Analytical chemistry*, 2009, **81**, 5188-5196.
100. H. V. Phan, T. Alan and A. Neild, *Analytical chemistry*, 2016, **88**, 5696-5703.
101. C. Lee, J. Lee, H. H. Kim, S.-Y. Teh, A. Lee, I.-Y. Chung, J. Y. Park and K. K. Shung, *Lab on a Chip*, 2012, **12**, 2736-2742.
102. F. Shen, Y. Li, Z.-M. Liu, R.-T. Cao and G.-R. Wang, *Chinese Journal of Analytical Chemistry*, 2015, **43**, 1942-1954.
103. M. Ryckelynck, S. Baudrey, C. Rick, A. Marin, F. Coldren, E. Westhof and A. D. Griffiths, *RNA*, 2015, **21**, 458-469.
104. C.-H. Chen, M. A. Miller, A. Sarkar, M. T. Beste, D. A. Lauffenburger, L. G. Griffith and J. Han, 2012.
105. E. X. Ng, M. A. Miller, T. Jing, D. A. Lauffenburger and C. H. Chen, *Lab Chip*, 2015, **15**, 1153-1159.
106. E. Brouzes, M. Medkova, N. Savenelli, D. Marran, M. Twardowski, J. B. Hutchison, J. M. Rothberg, D. R. Link, N. Perrimon and M. L. Samuels, *Proceedings of the National Academy of Sciences*, 2009, **106**, 14195-14200.
107. B. Xu, N.-T. Nguyen and T. Neng Wong, *Micro and Nanosystems*, 2011, **3**, 131-136.
108. J. Kamp, J. Villwock and M. Kraume, *Reviews in Chemical Engineering*, 2017, **33**, 1-47.
109. H. P. Kavehpour, *Annual Review of Fluid Mechanics*, 2015, **47**, 245-268.
110. J. S. Eow, M. Ghadiri, A. O. Sharif and T. J. Williams, *Chemical Engineering Journal*, 2001, **84**, 173-192.
111. D. J. Im, *Korean Journal of Chemical Engineering*, 2015, **32**, 1001-1008.
112. W. Wang, C. Yang and C. M. Li, *Lab on a Chip*, 2009, **9**, 1504-1506.
113. C. Priest, S. Herminghaus and R. Seemann, *Applied Physics Letters*, 2006, **89**, 134101.
114. X. Niu, F. Gielen, A. J. deMello and J. B. Edel, *Analytical Chemistry*, 2009, **81**, 7321-7325.
115. Z. Liu, S. T. Chan, H. A. Faizi, R. C. Roberts and H. C. Shum, *Lab on a Chip*, 2015, **15**, 2018-2024.
116. M. Mannoor, S. Kang and Y. K. Suh, *Advances in Condensed Matter Physics*, 2015, **2015**, 9.
117. A. J. T. Teo, S. H. Tan and N.-T. Nguyen, *Analytical Chemistry*, 2019.
118. M. Zagnoni, G. Le Lain and J. M. Cooper, *Langmuir*, 2010, **26**, 14443-14449.
119. M. Lee, J. W. Collins, D. M. Aubrecht, R. A. Sperling, L. Solomon, J.-W. Ha, G.-R. Yi, D. A. Weitz and V. N. Manoharan, *Lab on a Chip*, 2014, **14**, 509-513.
120. B. Bhattacharjee and S. A. Vanapalli, *Biomicrofluidics*, 2014, **8**, 044111.
121. A. Ray, V. B. Varma, P. Jayaneel, N. Sudharsan, Z. Wang and R. V. Ramanujan, *Sensors and Actuators B: Chemical*, 2017, **242**, 760-768.
122. A. Ghaffari, S. H. Hashemabadi and M. Bazmi, *Colloids and Surfaces A: Physicochemical and Engineering Aspects*, 2015, **481**, 186-198.
123. V. Misuk, A. Mai, K. Giannopoulos, F. Alobaid, B. Epple and H. Loewe, *Lab on a Chip*, 2013, **13**, 4542-4548.

124. S. Afkhami, A. Tyler, Y. Renardy, M. Renardy, T. S. Pierre, R. Woodward and J. Riffle, *Journal of Fluid Mechanics*, 2010, **663**, 358-384.
125. V. B. Varma, A. Ray, Z. M. Wang, Z. P. Wang and R. V. Ramanujan, *Scientific reports*, 2016, **6**, 37671.
126. A. Ray, V. B. Varma, Z. Wang, Z. Wang, P. Jayaneel, N. M. Sudharsan and R. V. Ramanujan, *IEEE Magnetics Letters*, 2016, **7**, 1-5.
127. J.-P. Huang, X.-H. Ge, J.-H. Xu and G.-S. Luo, *Chemical Engineering Science*, 2016, **152**, 293-300.
128. J. Köhler, T. Henkel, A. Grodrian, T. Kirner, M. Roth, K. Martin and J. Metze, *Chemical Engineering Journal*, 2004, **101**, 201-216.
129. B. Xu, N.-T. Nguyen and T. N. Wong, *Biomicrofluidics*, 2012, **6**, 012811.
130. T.-D. Luong, N.-T. Nguyen and A. Sposito, *Applied Physics Letters*, 2012, **100**, 254105.
131. C. N. Baroud, M. R. de Saint Vincent and J.-P. Delville, *Lab on a Chip*, 2007, **7**, 1029-1033.
132. S. S. Dixit, H. Kim, A. Vasilyev, A. Eid and G. W. Faris, *Langmuir*, 2010, **26**, 6193-6200.
133. D. H. Yoon, A. Jamshaid, J. Ito, A. Nakahara, D. Tanaka, T. Akitsu, T. Sekiguchi and S. Shoji, *Lab on a Chip*, 2014, **14**, 3050-3055.
134. A. Jamshaid, M. Igaki, D. Yoon, T. Sekiguchi and S. Shoji, *Micromachines*, 2013, **4**, 34-48.
135. Z.-X. Guo, Q. Zeng, M. Zhang, L.-Y. Hong, Y.-F. Zhao, W. Liu, S.-S. Guo and X.-Z. Zhao, *Sensors and Actuators A: Physical*, 2011, **172**, 546-551.
136. J. Dai, X. Yang, M. Hamon and L. Kong, *Chemical Engineering Journal*, 2015, **280**, 385-390.
137. M. Sesen, T. Alan and A. Neild, *Lab on a Chip*, 2014, **14**, 3325-3333.
138. S. B. Kim and S. S. Kim, *JOSA B*, 2006, **23**, 897-903.
139. H. Cho, J. H. Jung and H. J. Sung, *International Journal of Heat and Fluid Flow*, 2015, **56**, 324-334.
140. J. H. Jung, K. H. Lee, G. Destgeer, K. S. Lee, H. Cho, B. H. Ha and H. J. Sung, *Microfluidics and Nanofluidics*, 2015, **18**, 1247-1254.
141. L. Nurdin, A. Venancio-Marques, S. Rudiuk, M. Morel and D. Baigl, *Comptes Rendus Chimie*, 2016, **19**, 199-206.
142. A. Diguet, H. Li, N. Queyriaux, Y. Chen and D. Baigl, *Lab on a Chip*, 2011, **11**, 2666-2669.
143. P. Dunkel, Z. Hayat, A. Barosi, N. Bchellaoui, H. Dhimane, P. I. Dalko and A. I. El Abed, *Lab on a Chip*, 2016, **16**, 1484-1491.